

We are IntechOpen, the world's leading publisher of Open Access books Built by scientists, for scientists

6,900

Open access books available

186,000

International authors and editors

200M

Downloads

Our authors are among the

154

Countries delivered to

TOP 1%

most cited scientists

12.2%

Contributors from top 500 universities



WEB OF SCIENCE™

Selection of our books indexed in the Book Citation Index
in Web of Science™ Core Collection (BKCI)

Interested in publishing with us?
Contact book.department@intechopen.com

Numbers displayed above are based on latest data collected.
For more information visit www.intechopen.com



Si Nanocrystal Arrays Created in SiO₂ Matrix by High-Energy Ion Bombardment

Irina Antonova

*A.V. Rzhanov Institute of Semiconductor Physics SB RAS
Russia*

1. Introduction

In the next two decades, nanoscience and nanotechnologies will transfer into new products and processes. One emerging area where this challenge will be successfully met is the field of semiconductor nanocrystals (NCs) (see, for instance, Norris et al., 2008). The promises offered by dielectric layers with hosted semiconductor nanocrystals in applications include production of silicon-based light emitting systems (Iacona et al., 2006), wavelength-tunable lasers (Klimov et al., 2007), memory elements (Hu et al., 2009), solar cells (Gur et al., 2008), low-dimensional devices (for instance, single electron transistors operating at room temperature (Zhou et al., 2010)), and a wide spectrum of biotechnologies (for instance, bioimaging (Michalet et al., 2005)). The prospects for developing new electronic and optoelectronic devices on the basis of spatially ordered arrays of quantum dots (QDs) embedded in a semiconductor or insulator matrix have arouse currently growing interest in the production methods of such arrays and in the studies of their optical and electronic properties.

The idea to use non-overlapping tracks of high-energy ($E \geq 1$ MeV/amu) heavy ions for production of nanocrystalline (NC) systems is becoming increasingly attractive among the various methods for fabrication of nanodimensional structures (nanolithography, molecular nanoelectronics, organic nanostructures, etc.) (Fink et al., 2007; Rizza et al., 2009). Beams of heavy fast ions can be efficiently used not only for formation, but also for modification, of nanodimensional structures, in particular, metallic nanoclusters (Klaumunzer, 2006; D'Orleans et al., 2003). Avasthi et al. (Avasthi et al., 2010) have summarized experimental data on the formation of elongated metal nanoparticles, and suggested a model for the interaction of fast ions with such nanoparticles dependently on nanoparticle sizes. Studies of the effect of high-energy ion irradiation on the formation of semiconductor (silicon or germanium) nanoclusters have also appeared recently (Chaudhari et al., 2003; 2005; Arnoldbik et al., 2005). It was shown that, as a consequence of the high density of ionization energy losses in the material, silicon nano-inclusions could be formed in SiO_x layers without any additional thermal treatment given to the samples. Studies of the effect of high-energy ion irradiation on SiO₂ layers containing Si nanocrystals or an excess concentration of dissolved silicon (Si:SiO₂ layers) have made it possible to propose a new approach to formation of vertically ordered NC arrays (Antonova et al., 2008 a; 2009 a; 2009 b; 2010 a; 2010 b).

In the present review, we demonstrate the possibility of using irradiation of samples with high-energy gas ions (Kr, Xe, and Bi) for introduction and modification of Si nanocrystals in Si:SiO₂ and NC:SiO₂ layers, and also for formation of ordered arrays of Si nanocrystals embedded in a SiO₂ matrix. Due to the small size of nanocrystals synthesized in our samples (typically, $\leq 6 - 8$ nm), in describing our results we will also use an alternative term 'quantum dots'. We will analyze the changes in the optical and electronic properties of NC systems and discuss possible applications of such systems. It should be emphasized here that a special feature of used irradiation, in contrast to conventional ion implantation, is huge ion-energy losses in the bulk of Si:SiO₂ layers and simultaneous creation of a relatively low defect concentration in such layers (Antonova et al., 2006a; Toulemonde et al., 2000; Meftah et al., 1997). The factor causing a low defect concentration in examined irradiated layers is the small thickness of those layers, which is normally much smaller than the projected ion range. Hence, while in practice defects are introduced in the substrate of film systems, the energy is mainly dissipated in the top Si:SiO₂ layer. The latter circumstance has allowed us to separate out the positive effect of ion irradiation (the huge energy losses in ion tracks) from the negative effect (defect formation).

2. Sample preparation and ion irradiation conditions

2.1 Nanocrystals in SiO₂ layers with varied concentration of excess Si

The Si:SiO₂ layers of thickness 400–1000 nm used in our study were sputtered from Si and SiO₂ sources onto silicon substrates. In the experimental arrangement used, the SiO₂ and Si sources were spaced ~ 100 mm apart. The large distance between the sources provided a possibility to form layers with varied concentration of excess silicon in the oxide. After annealing of samples and formation of nanocrystals, we could obtain layers with concentration and sizes of NCs varied in the lateral plane. That gave us an interesting opportunity to examine the properties of formed Si:SiO₂ layers as dependent on NC concentration and sizes. The excess Si content of the silicon-rich oxide layers ranged from 4 to 94 vol.%. The composition of deposited layers was estimated from the thickness of Si and SiO₂ layers obtained by individual deposition of films from the Si and SiO₂ sources onto different substrates (Shamin et al., 2010). Subsequent high-temperature annealing (at 1140°C for 40 min) used for part of samples resulted in the formation of silicon oxide layers containing Si nanocrystals (NC:SiO₂ layers), whose sizes only slightly depended on layer composition and whose concentration increased with coordinate along the sample by several orders of magnitude (Sa'ar et al., 2005; Antonova et al., 2006b). Experimental results are presented below as a function of excess Si concentration. This parameter is used to characterize the composition of our Si:SiO₂ layers since its value was inherently defined by the evaporation procedure, whereas other parameters, such as NC concentration and sizes, were complicated functions of layer composition, and also of thermal treatments given to the samples.

2.2 High-energy ion irradiation: Specific features

For irradiation of Si:SiO₂ and NC:SiO₂ layers obtained as described above, Kr, Xe, or Bi ions respectively with energies 90, 130–250, and 65–670 MeV were used. The ion fluences ranged from 3×10^{11} to 3×10^{13} cm⁻². The irradiations of our samples were performed with the use of accelerators available in the Laboratory of Nuclear Reactions, Joint Institute for Nuclear

Research, Dubna. For the ion energies used, the ion penetration range was 15–23 μm (see Table 1); i.e. it was substantially larger than the thickness of silicon-rich oxide layers. This means that almost all ions penetrated into the substrate, and the defects generated in elastic scattering channels were also predominantly introduced in the substrate, whereas prevailing energy losses in the layers were the electron stopping losses.

With reference to SRIM data, the electron stopping losses due to ionization dE_e/dx in the oxide layers were expected to vary from 7.1 (Kr), 10.2 (Xe), and 22.0 keV/nm (Bi) for the SiO₂ end of the sample to 9.5 (Kr), 12.3 (Xe), and 24.3 keV/nm (Bi) for its Si end. The ionization losses of ion energy lead to ionization of atoms in the material under irradiation. In a time interval of 10^{-13} - 10^{-12} s the excitation energy was transferred into anisotropic heating of the oxide layers due to thermalization process. Using the value of ionization losses, the dependence of ion-track sizes in α -SiO₂ on ion energy, and the thermal spike model of (Toulemonde et al., 2000; Meftah et al., 1997), we could estimate the width of ion tracks in our samples, which turned out to be about 4-6 nm. Results for the time evolution of temperature inside ion tracks calculated by TSRIKE-02 software (Toulemonde et al., 2000) are shown in Fig.1a. TSRIKE-02 simulates the electron-lattice interaction (transfer of the ionization losses of ions into the heating of the target lattice). The variable parameter of the ion-lattice interaction is the radius of the shells surrounding individual ion trajectories in which the main portion of ion energy is lost for ionization. As it follows from Fig.1a (see also Fig.15 a), the local transient temperature in ion track cores in our experiments could reach 1700 - 2500°C, the ion-track heating time being about 10^{-11} - 10^{-10} s. It means that almost all inter-atomic bonds along ion tracks could be broken to free the atoms and make them capable of displacing from their regular lattice sites. As a result, new bonds could readily form in the material, this process leading to subsequent amorphization or crystallization of part of previously existing Si nanoparticles as well as to the formation of new NCs in the oxide layer along ion tracks.

One more effect that was taken into consideration for materials subjected to the irradiation with high-energy ions (see also Section 6) is ion-beam-induced anisotropic plastic deformations (Van Dillen et al., 2004; 2005). The strain anisotropy is imposed by the direction of the ion beam: normally, the material expands in the direction normal to the ion beam and contracts parallel to it, while maintaining their volume. According to the developed model, the strain ε (determined as the relative change of lattice constant) versus time goes through a maximum and then reaches a constant value. The anisotropic strain rises with ion energy and fluence. It should be emphasized here that up to fluences 10^{12} cm⁻² the ion tracks in the material were independent of each other, whereas at higher fluences they can become overlapping.

The ionization losses of the ions and the anisotropic heating of the material are higher in Si in comparison with SiO₂. The anisotropic deformations found in amorphous silicon are typically 1.5 orders of magnitude lower than the anisotropic deformations in SiO₂ (Van Dillen et al., 2005; Meftah et al., 1997). This means that the anisotropic strain and the anisotropic heating should demonstrate considerable changes with increasing concentration of Si nanocrystals embedded in the SiO₂ layer. In the case of variable NC concentration we have to expect a strong anisotropic-strain effect for SiO₂ layers with low Si-phase content and a more pronounced anisotropic heating effect for SiO₂ layers with high excess Si phase content.

Sample, thickness of SiO _x layer, nm	Annealing regime before irradiation	Ion energy, MeV	Fluence, cm ⁻²	R _p in Si, nm	ΔE _e /Δx, keV/nm	Annealing after irradiation
NC-10, 700	1140°C, 40 min					
NC-11, 700	1140°C, 40 min	Kr, 90	1x10 ¹²	16	7.1	
NC-11a, 700	1140°C, 40 min	Kr, 90	1x10 ¹²	16	7.1	800°C, 20 min
NC-20, 1000	1140°C, 40 min					
NC-21, 1000	1140°C, 40 min	Kr, 90	1x10 ¹²	16	7.1	-
NC-22, 1000	-	Xe, 130	1x10 ¹²	17	10.2	1140°C, 40 min
NC-23, 1000	1140°C, 40 min	Xe, 130	1x10 ¹²	17	10.2	
NC-23a, 1000	1140°C, 40 min	Xe, 130	1x10 ¹²	17	10.2	800°C, 20 min
NC-24, 1000	1140°C, 40 min	Xe, 130	1x10 ¹³	17	10.2	800°C, 20 min
NC-30, 400	1140°C, 40 min					
NC-31, 400	1140°C, 40 min	Kr, 250	1x10 ¹²	33.1	10.2	
NC-31a, 400	1140°C, 40 min	Kr, 250	1x10 ¹²	33.1	10.2	800°C, 20 min
NC-32, 400	1140°C, 40 min	Kr, 250	2x10 ¹³	33.1	10.2	
NC-32a, 400	1140°C, 40 min	Kr, 250	2x10 ¹³	33.1	10.2	800°C, 20 min
NC-33, 400	1140°C, 40 min	Bi, 65	1x10 ¹²	10	8.9	800°C, 20 min
NC-34, 400	1140°C, 40 min	Bi, 130	1x10 ¹²	16	13.2	800°C, 20 min
NC-35, 400	1140°C, 40 min	Bi, 670	3x10 ¹¹	43	18.0	800°C, 20 min
NC-36, 400	1140°C, 40 min	Bi, 670	1x10 ¹²	43	18.0	800°C, 20 min
NC-37, 400	1140°C, 40 min	Bi, 670	8x10 ¹²	43	18.0	800°C, 20 min
NC-38, 400	1140°C, 40 min	Bi, 670	3x10 ¹³	43	18.0	800°C, 20 min

Table 1. Parameters of structures used, and annealing and irradiation regimes. R_p is the projected ion range in Si calculated by SRIM. ΔE_e/Δx values are the ionization losses of the ions in SiO₂.

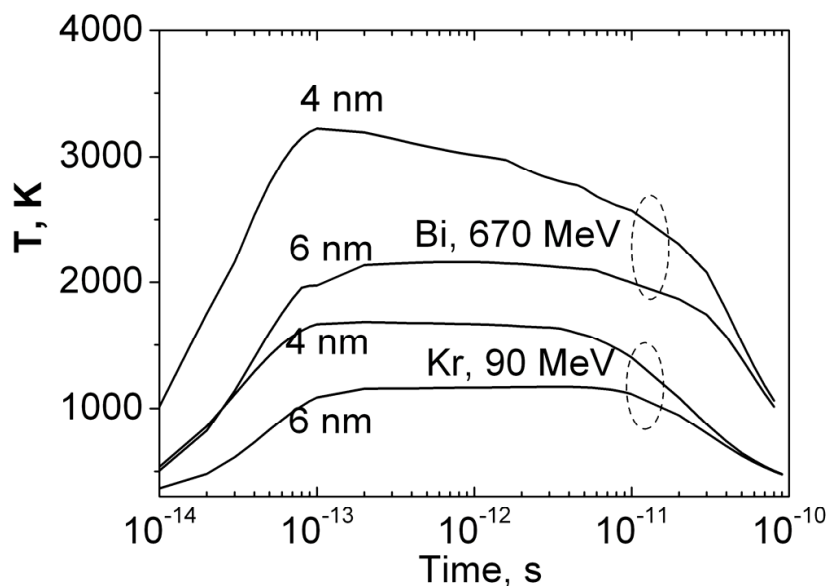


Fig. 1. Simulated evolution of temperature in time in α -SiO₂ (quartz) samples for increasing radial distances from the ion track axis. The simulations were performed using the TSPIKE-02 software (Toulemonde et al., 2000). For times shorter than 10⁻¹³ sec the temperature should be considered as quasi-temperature.

3. Structural modification of Si nanocrystals embedded in SiO₂ matrix

3.1 Ordered nanocrystal arrays in ion-modified layers

In the initial (non-irradiated) layers, the spherically shaped Si nanocrystals were distributed randomly over the insulator matrix; the NC spheres were 3–5 nm in diameter for excess Si contents of Si:SiO₂ layers 40–70 vol.%, with the atomic planes in the nanocrystals having random orientation. After ion irradiation with ionization losses over 6 keV/nm, in the oxide layers with a relatively high excess Si content (above 35%) vertically ordered NC arrays were formed along ion tracks (Fig.2) (Antonova et al., 2009 a; 2009 b). The morphology of NCs has also changed: the nanocrystals became extended along the ion tracks. As shown in Fig. 2 b, this effect is accompanied by another effect: the atomic planes in the formed NCs were aligned in the direction along ion tracks, with deviation $\pm 20^\circ$. It should be emphasized here that no other method of forming Si NCs allows production of vertically ordered arrays of nanocrystals with identically oriented atomic planes.

The TEM images presented in Fig.2 were obtained for samples NC-11 and NC-21 irradiated with 90 MeV Kr ions; the excess Si content of the oxide layer in those samples was 37–45%. The Kr ion had a minimal mass and a relatively low energy. We believe that in the case of using for irradiation heavier ions with a higher energy such effects will become essentially more pronounced.

In irradiated Si:SiO₂ structures which initially contained no NCs (sample NC-22), introduction of Si nanocrystals with a similar spatial and size distribution was revealed after additional high-temperature thermal treatments given to the samples.

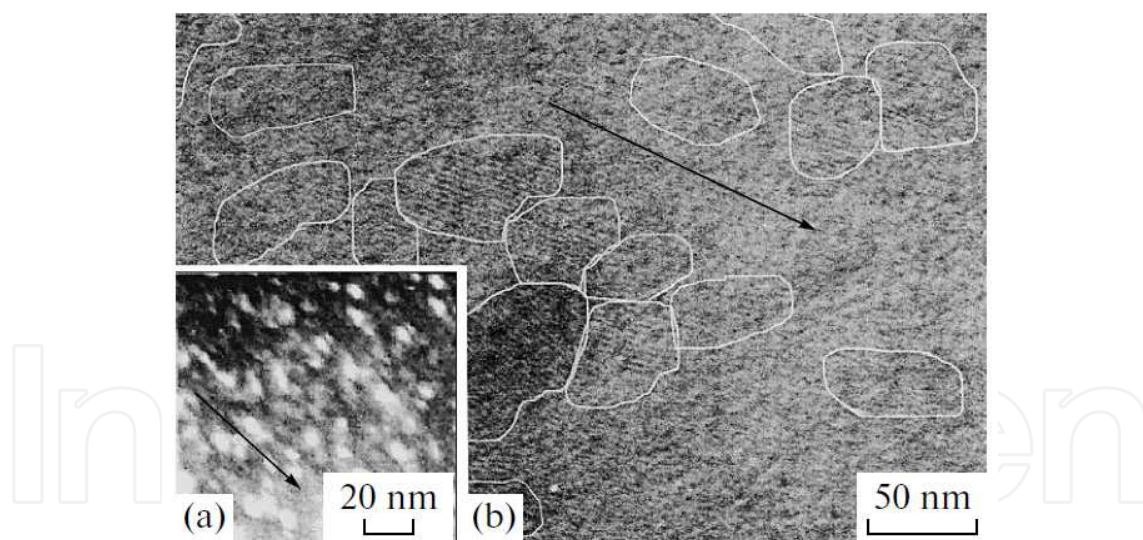


Fig. 2. Cross-sectional TEM and HRTEM images of NC:SiO₂ layers in samples NC-21 irradiated with 90 MeV Kr ions to a fluence of 10^{12} cm⁻². The Si phase contents of the samples were about 37 (a) and 73 vol.% (b). The arrows show the direction of ion tracks. Note that in the irradiated sample (b) the atomic planes inside nanocrystallites are aligned along ion tracks (with deviation $\pm 20^\circ$).

3.2 Amorphization and crystallization processes studied by Raman spectroscopy

Figure 3 a, b compares Raman spectra taken from initial and irradiated samples in areas with two different Si-content values, 51% and 62% (Antonova et al., 2009 a; 2010 a). The

Raman line due to the single-crystal Si substrate is detected at 521 cm^{-1} . After the samples were irradiated with Kr or Bi ions, the amorphous 480 cm^{-1} line has increased significantly. In the case of Bi irradiation, an NC-related line at $500\text{--}520\text{ cm}^{-1}$ was also observed in the spectra. To demonstrate this effect, we have plotted in Fig. 2a the difference between the spectrum of a sample irradiated with Bi ions and the spectrum of the same sample before irradiation. An NC-related peak at $500\text{--}520\text{ cm}^{-1}$ is also observed in the differential spectrum; this fact points to the formation of new NCs in samples subjected to irradiation. An increase in the irradiation dose ($> 10^{12}\text{ cm}^{-2}$) and a decrease in ion energy and/or ion mass lead to domination of the amorphization process. Raman measurements performed on samples with higher Si contents ($> 70\text{ vol.}\%$) have shown that, in the latter case, only amorphization of Si NCs was observed. Following an additional anneal at 800°C for 20 min, no substantial changes were observed in the Raman spectra.

It was found that irradiation of Si:SiO₂ structures that initially contained no previously formed NCs also brought about the formation of new Si nanocrystals in the course of irradiation. This effect was observed practically for all ions used in the present study. In this case, the formation of new nanocrystals also prevails at relatively low Si contents of Si:SiO₂ layers (below 50–60%), whereas the formation of amorphous inclusions prevails at higher Si contents. An increase in irradiation dose (over 10^{12} cm^{-2}) and a decrease in the specific ionization losses of the ions yield a net increase in the amount of optically active nanocrystals available in the samples (Antonova et al., 2010 b).

3.3 Evolution of NC sizes under ion irradiation

It was also shown that a study of Si NCs by means of charge deep-level transient spectroscopy (Q-DLTS) makes it possible to observe the capture of charge carriers by, and their emission from, dimensional quantization levels in NCs located close to the SiO₂/Si interface (Antonova et al., 2009 c; 2011). The Q-DLTS method was also employed to investigate into variations of energy barriers involved in the emission process of charge carriers from NC levels in NC:SiO₂ layers modified with high-energy ion irradiation.

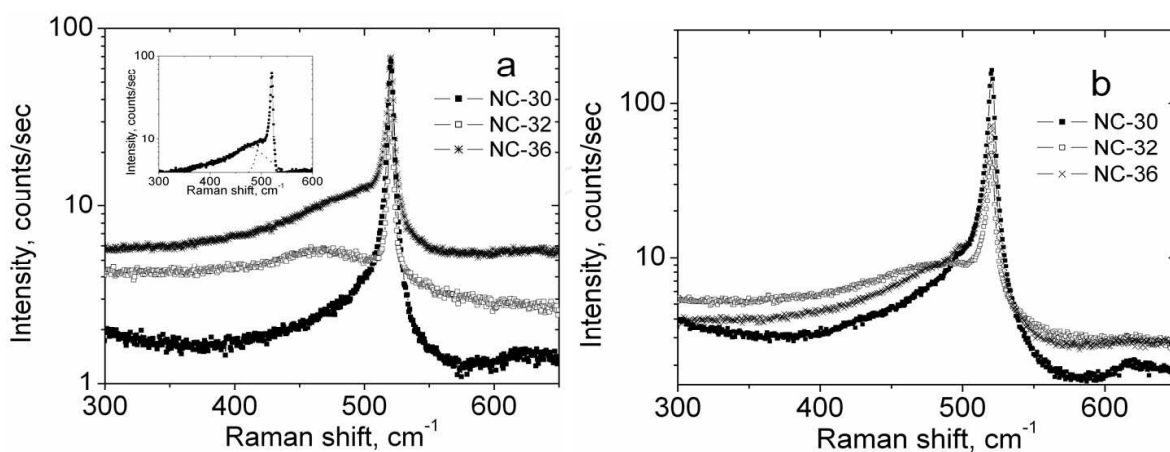


Fig. 3. Raman spectra of NC-SiO₂ layers on Si substrates for initial (non-irradiated) samples with (a) 51% and (b) 62% of the Si phase and for samples irradiated with Kr (NC-32) and Bi ions (NC-36). In order to demonstrate the added intensity around the "amorphous" 480 cm^{-1} line and the NC-related $500\text{--}520\text{ cm}^{-1}$ line due to Bi⁺ irradiation, in the insert to the figure we have plotted the difference between the spectra measured after and before the irradiation of the sample with 670 MeV Bi⁺ ions (NC-30 and NC-36).

Samples NC-36 and NC-37 to be discussed in the present section were irradiated with Bi ions of about 670 MeV energy (the projected ion range 43 nm) to fluences in the range 10^{12} – 10^{13} cm⁻². Those ions, having a maximal mass and energy, were expected to provide the most significant effect on Si NCs. The specific ionization losses of 670 MeV Bi ions in the SiO₂ layers were 24 keV/nm, which value far exceeded the threshold ionization energy (~2 keV/nm) required for the formation of latent tracks in SiO₂ (Toulemonde et al., 2000). Prior to performing Q-DLTS measurements, the radiation defects introduced in the substrate were removed from it giving the samples an additional anneal at 800°C during 20 min.

As a rule, Q-DLTS spectra of non-irradiated and irradiated samples involved a single peak. In the temperature range 80 to 300 K, this peak features two slopes in the Arrhenius dependence (Fig. 4a). The activation energies determined from the measurements made at several points on a sample with different compositions of the NC:SiO₂ layer are listed in Table 2. A hypothesis was put forward that the levels detected by Q-DLTS in the NC:SiO₂ layers were quantum confinement levels in Si nanocrystals. In the latter case, the energy interval between the levels could be expected to be dependent on NC sizes. Assuming that $\Delta E_i = E_{n=2} - E_{n=1}$ (here, $E_{n=2}$ and $E_{n=1}$ are the energies of the first excited and ground state of an electron in the quantum dot), we were able to evaluate the typical NC size value W from the theoretical relation between E_n and W . Starting with the effective mass approximation (Moskalenko et al., 2007), we have obtained, from the theoretically estimated values of ΔE_i , the W values given in the last column of Table 2. Trying then to approximate the dependence $E_n(W)$ with the simpler well-known expression (see, for example, Gaponenko, 1998),

$$E_n = \frac{\hbar^2}{2m} \cdot \left(\frac{\pi^2}{W} \right) \cdot n^2, \quad (1)$$

where E_n is the energy of the n -th confined level and m is the electron effective mass in crystalline Si (0.26 in units of the free electron mass), we have obtained W values given in the last column of the table as bracketed values. We see that the estimated values of W fall into the 3-6 nm range for the reference (non-irradiated) sample NC-30. These values of W show a good correlation with TEM data. Q-DLTS measurements yield practically identical sets of levels for various points measured along samples, this finding being in turn indicative of an identical set of NC sizes. As it follows from Table 2, the irradiation brings about a decrease of NC sizes. A further decrease in NC sizes was observed in samples irradiated to higher fluences. In the latter case, formation of smaller Si nanocrystals might proceed due to three different reasons. The first reason is the formation of new small Si nanocrystals in the samples under irradiation. The second reason is possible decrease in the sizes of already existing NCs, which could be a result, for instance, of oxidation of the nanocrystals. It should be noted here that dissolution of metallic nano-inclusions (in particular, Au inclusions) in samples irradiated with high-energy ions was observed by Rizza et al. (Rizza et al., 2007 a; 2007 b). The third reason, operating in a situation in which the shape of NCs could be altered by ion irradiation from spherical to ellipsoidal one, extended along ion tracks, is that the energies of quantum confinement levels were primarily defined by the smallest NC size. In the latter case, a decrease in NC sizes could be indicative of an elongation of nanocrystals and of a decrease of their effective diameter. Photoluminescence (PL) measurements performed on the same structures yields for the blue

shift of the NC-related PL peaks observed in the spectrum (see Section 4.1) a value consistent with the decrease of NC sizes as estimated from Q-DLTS data.

Figure 4 b shows the density of deep traps detected by Q-DLTS as a function of the composition of the NC:SiO₂ layer. It is seen that, as a result of ion irradiation, the trap density has decreased by approximately one order of magnitude. The decrease in the density of nanocrystals detected by the Q-DLTS method in irradiated samples in comparison with pristine samples NC-30 correlates with the formation of conducting NC chains in ion tracks, which phenomenon will be discussed in more detail below. Only isolated Si nanocrystals located in the outside region of conducting chains and being therefore able to retain charge made a contribution to the Q-DLTS signal.

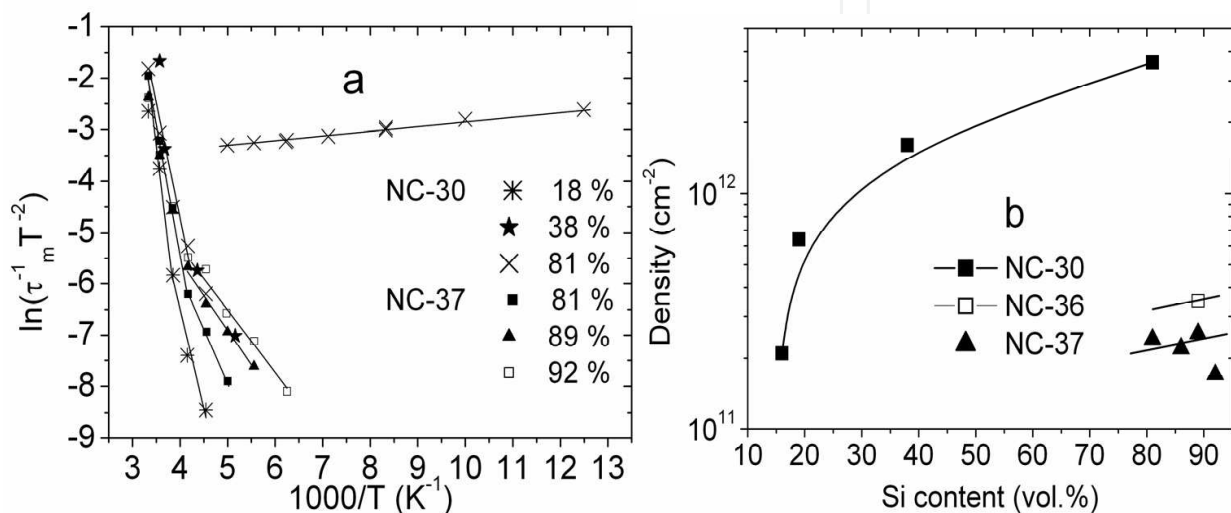


Fig. 4. (a) Arrhenius plots for Q-DLTS peaks measured in regions with different Si-phase contents along the initial (non-irradiated) sample NC-30 and along the sample NC-37, whose NC:SiO₂ layer was modified by irradiation of the sample with Bi ions. (b) The sheet concentration (density) of traps in the NC:SiO₂ layers versus the Si-phase content of these layers for three sets of samples, NC-30, NC-36 and NC-37.

A schematic energy diagram of a nanocrystal embedded within a SiO₂ matrix in a vicinity of the substrate is shown in Fig.5 for the regime of capture of charge carriers by NCs during Q-DLTS filling pulse (a) and for the regime in which the emission process is observed (b). A higher energy position of dimensional-quantization levels in the nanocrystal in comparison with the edge of the conduction band of silicon and an additional increase in the energy of the levels by the energy of NC charging with electrons suggest that, here, direct tunneling of NC-emitted charge carriers into the Si substrate is possible. The observation of NC-related levels by the Q-DLTS method and the evaluation of the activation energies related to the emission of charge carriers from NCs into substrate show that the emission process could proceed due to a combination of thermal activation and tunneling processes. The latter is possible if the emission of charge carriers proceeds via some intermediate level E^* available at the NC/SiO₂ interface. In such a situation, the activation energies experimentally determined from the treated Q-DLTS spectra present the energy differences $E^* - E_i$. The presence of an intermediate level E^* at the NC/SiO₂ interface was often postulated in interpretation of NC-related photoluminescence (e.g. Godefroo et al., 2006). The fact that the activation energy for the emission of charge carriers from NCs proved to be practically

invariable with a strong increase of excess Si content in our samples suggests that the role of the matrix is not too much important. This suggests that the level E^* involved in the tunneling process was located at the NC/matrix interface rather than at the interface between the SiO₂ layer and the Si substrate. Most likely, in real samples Si nanocrystals embedded within the SiO_x matrix are coated with a SiO₂ shell.

From the position of the Q-DLTS peak in the Q-DLTS spectra, the characteristic time of emission of charge carriers from NC-related levels could be estimated. Figure 6 shows the temperature dependences of this time. Comparing the data shown in Fig.5 for the initial and irradiated samples, we may conclude that the substantial rearrangement in the NC system having occurred as a result of ion irradiation of the samples had no appreciable effect on the characteristic times of recharging of individual isolated nanocrystals in the temperature range from 220 to 300 K; those times amounted to 10⁻²-10⁻⁴ s. On the average, at lower temperatures the times of emission of charge carriers from NC levels in irradiated samples proved to be shorter than the same times in pristine structures.

The average values of the activation energies for emission of charge carriers from nanocrystals in non-irradiated samples were found to be $E^* - 0.24$ and $E^* - 0.43$ eV. After irradiation with ions to a fluence 10¹² cm⁻², those energies have decreased to $E^* - 0.13$ and $E^* - 0.35$ eV and, as the fluence was further increased, those energies have further decreased to $E^* - 0.11$ and $E^* - 0.34$ eV. It can be seen from a comparison of the values obtained that ion irradiation generally leads to a decrease in the activation energies. This decrease also

Samples	Si content, vol. %	E_a , eV	ΔE_i , eV	W, nm
NC-30	16	0.30 0.16	0.14	5.6 (3.6)
	19	0.43 0.24	0.19	4.8 (3.1)
	38	0.43 0.23	0.20	4.7 (3.0)
	81	0.43 0.27 0	0.16	5.1 (3.3)
NC-36 Bi, 670 MeV, 1x10 ¹² cm ⁻²	89	0.35 0.13	0.22	4.4 (2.7)
NC-37 Bi, 670 MeV, 8x10 ¹² cm ⁻²	82	0.44 0.12	0.32	3.6 (2.3)
	87	0.37 0.03	0.34	3.3 (2.0)
	89	0.33 0.10	0.23	4.3 (2.6)
	92	0.43 0.10	0.33	3.6 (2.2)

Table 2. The energies of deep traps E_a as extracted from the Q-DLTS spectra of samples with different Si contents of the NC:SiO₂ layer. The ΔE_i values are the energy separations between the levels E_a for a given Si content. Also indicated in the table are the quantum-dot sizes (diameters), W, as estimated through comparison of experimentally determined ΔE_i values with the theoretical predictions of ref. (Moskalenko et al., 2007) and from formula (1) (bracketed values).

manifests itself as a decrease of the emission times for charge carriers at relatively low temperatures. A decrease in the activation energy can be attributed to a decrease in NC sizes, or to an increase in the energies of dimensional quantization levels.

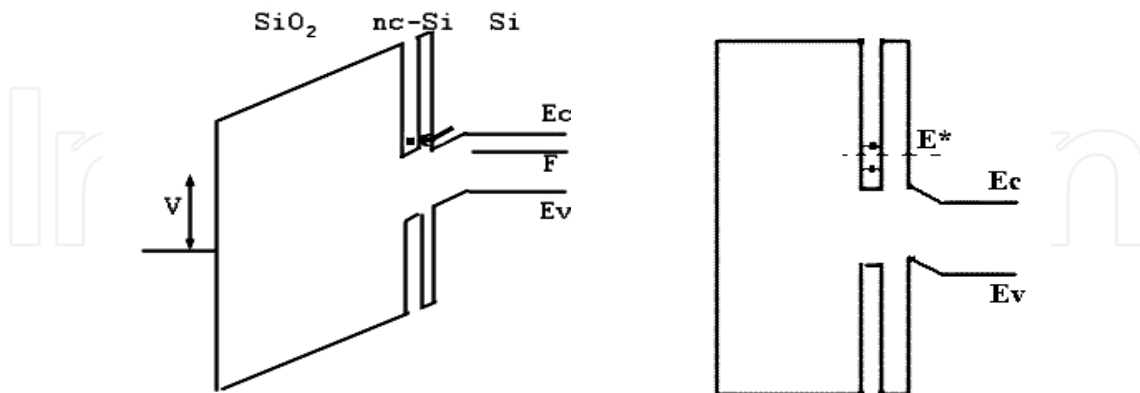


Fig. 5. Energy diagrams illustrating the NC charging process (left) and the process of electron emission from NC-related levels (right) observed during and after the filling pulse in the Q-DLTS procedure. For simplicity, only one NC, located in the vicinity of the SiO_x/Si substrate interface, is depicted in the diagrams.

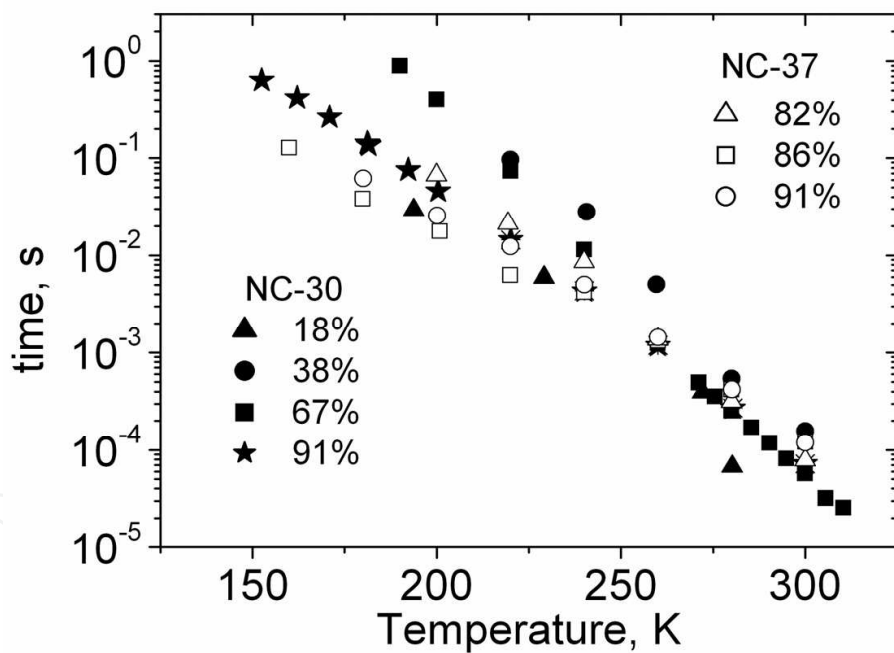


Fig. 6. Temperature dependence of the characteristic time of emission of charge carriers from quantum confinement levels in nanocrystals for samples NC-30 and NC-37. The emission time for sample NC-36 has intermediate values.

4. Optical and electrical properties of ion-modified arrays of nanocrystals

4.1 Photoluminescence of irradiated NC arrays

The capability of Si nanocrystals to emit light in the visible spectral region attracts a lot of interest, thus stimulating the studies of the optical properties of NC systems aimed at

enhancement of the PL intensity coming from nanocrystals. For the initial (non-irradiated) NC-SiO₂ layers it was found that the PL signal due to NCs could be observed only in a certain range of layer compositions (Fig. 7 a). The PL intensity decreased with increasing concentration of Si NCs (or excess Si content of NC-SiO₂ layers) when the nanocrystals started to cluster together and, thereafter, percolation conduction appeared in the NC system (Antonova et al., 2006 b; 2008 b). The possibility of migration of charge carriers over extended NC clusters substantially diminishes the probability of radiative recombination of electrons and holes optically generated in NCs, thus resulting in a decreased PL intensity.

The electronic losses of the ions being relatively low (Kr, 90 MeV, $dE_e/dx = 7.1$ keV/nm), the ion irradiation induces no substantial changes in the PL intensity coming from NC-SiO₂ layers (Fig. 7 a, NC-10, NC-11) (Antonova et al., 2008 a). Following irradiation, an insignificant change in the spectral position of the NC-related PL peak was only observed (see Fig. 7 b). We have suggested that such a change could be a result of a change of NC sizes. The higher was the Si content of the NC-SiO₂ layers, the larger NCs were observed in such layers after ion irradiation. As estimated from the position of the PL peak in the spectrum and from the relation of the latter position with typical NC sizes in the NC systems (see Bitten et al., 2004), the average size of Si nanocrystals in sample NC-10 before irradiation was 3.6 nm. The latter value well correlates with the NC sizes that were estimated from Raman measurements and TEM observations. After ion irradiation (sample NC-11), based on the blue shift of the NC-related PL peak the typical NC size could be estimated as 3.5 nm for 27% and 3.9 nm for 57% Si content of NC-SiO₂ layer. It should be noted here that an additional peak at about 570 nm appeared in the PL spectra of irradiated NC-SiO₂ layers. This peak was attributed to the formation of small Si chains in irradiated samples (Kachurin et al., 1998).

Increase in the ionization losses of ions used for irradiation of samples (Xe, 130 MeV, $dE_e/dx = 10.2$ keV/nm) widened the range of compositions of the NC-SiO₂ layers for which an appreciable NC-related PL signal could be detected (Fig. 7 a, NC-22). Samples NC-23 and NC-23a exhibited PL spectra similar to the PL spectrum of sample NC-22. Here, the intensity of the NC-related PL decreases in value with increasing the Si content of NC-SiO₂ layer over 40 vol.% while a more intense photoluminescence was observed in samples with lower Si contents. The spectral position of the PL peak maximum observed in the PL spectra of examined samples is indicated in Fig. 7 a. It can be seen that the PL peak position exhibits a distinct blue shift with increasing Si content of the NC-SiO₂ layers. Observation of NC-related photoluminescence in part of samples with low Si contents points to the fact that, here, new nanocrystals were formed right during irradiation. An additional peak with a maximum located at about 550 nm was observed in irradiated samples. The observed blue shift in the spectral position of NC-related peaks points to the formation of an increased number of smaller Si NCs.

Further increase in ionization losses (Bi, 670 MeV, $dE_e/dx = 18$ keV/nm) demonstrates a possibility of reaching even greater PL intensity in NC systems irradiated with high-energy heavy ions (Antonova et al., 2009 a). The photoluminescence spectra that were taken from the reference sample NC-30 and from several irradiated samples with indicated Si content values are shown in Fig. 8 a. The NC-related PL peak in the reference sample NC-30 was observed at ~ 785 nm; the spectral position of this peak in the PL spectra of non-irradiated samples was roughly independent of the excess Si content of the Si:SiO₂ layers. In samples

irradiated with relatively low ion fluences (10^{12} cm $^{-2}$, sample NC-36 in Fig.8 b), a very strong increase in the PL intensity coming from NCs in the NC:SiO $_2$ layers was found, although the main spectral characteristics of the NC-related PL peak (spectral position and half-width) were the same as in the PL spectra of non-irradiated samples. Increase in the Bi ion fluence to 8×10^{12} cm $^{-2}$ (NC-37) leads to a very strong decrease of the registered PL intensity; simultaneously, there emerges a dependence of the spectral position of the NC-related PL peak on the excess Si content of the oxide layers. The data on the NC-related PL intensity considered as a function of the Si content of NC-SiO $_2$ layers are summarized in Fig. 8 d. These data suggest that an additional concentration of Si crystallites, resulting in PL intensity enhancement, could be formed in samples irradiated with relatively low ion fluence. Considering the data obtained in (Antonova et al., 2006 b; 2008 b), which show that the NC-related PL emission comes only from individual, geometrically isolated NCs, it can be inferred that in ion-irradiated NC:SiO $_2$ layer a high intensity of NC-related PL should be observed for relatively low excess Si contents of NC:SiO $_2$ layers. The PL quenching observed in the samples irradiated with higher ion fluences should be attributed either to formation of NC clusters or to amorphization of Si crystallites.

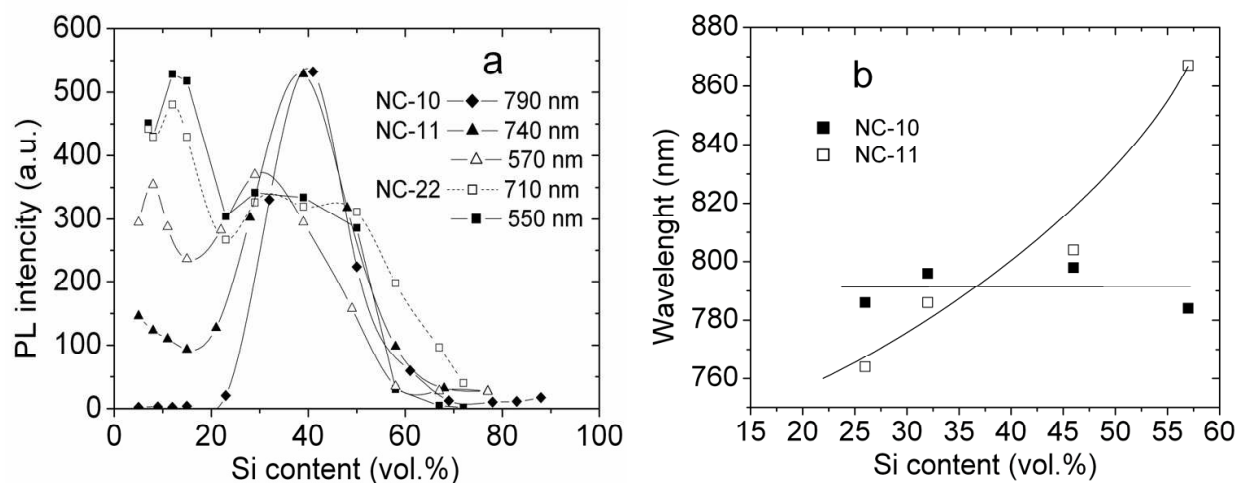


Fig. 7. (a) The dependence of the maximum PL intensity on the Si phase content in samples NC-10 and NC-11 irradiated with Kr ions; those samples contained a certain amount of Si NCs formed before irradiation. The sample NC-22 irradiated with Xe ions (10^{12} cm $^{-2}$) was subjected to a post-irradiation high-temperature anneal (1140°C, for 40 min). (Antonova et al., 2008 a) (b) Spectral position of the PL peak maximum in the PL spectra of samples NC-10 and NC-11 versus the Si content of the NC-SiO $_2$ layers.

The radiation effects observed in our samples can be summarized as follows:

- i. At fixed ion dose, in samples irradiated with ions producing relatively weak ionization in the material (Kr, ionization energy losses $dE_e/dx = 7.1$ keV/nm) and in samples irradiated with relatively high ion fluences ($\geq 8 \times 10^{12}$ cm $^{-2}$), the spectral position of the NC-related PL peak proved to be dependent on the excess Si content of the NC-SiO $_2$ layers. The effect was attributed to a change of NC sizes.
- ii. In the case of higher ionization losses (i.e. in the case of Xe and Bi ions with $dE_e/dx \geq 10.2$ keV/nm) the range of excess Si contents for which an intense NC-related PL was observed was found to be extended towards lower Si contents. A maximal PL intensity

was found in samples containing 17 – 20 vol.% of excess Si. The PL intensity in samples irradiated with low ion fluence ($\sim 1 \times 10^{12} \text{ cm}^{-2}$) could be a few times greater than the PL intensity coming from non-irradiated samples. Hence, at low fluence an efficient formation of NCs due to high-energy ion irradiation is observed in samples with relatively low Si content. Such a formation of Si NCs was found to occur both in silicon oxide layers with preliminarily formed NCs and in silicon oxide layers that contained just dissolved excess Si.

- iii. Increase in the ion fluence quenches the NC-emitted PL due to formation of extended NC clusters in the NC-SiO₂ layers and/or due to amorphization of already formed Si crystallites.

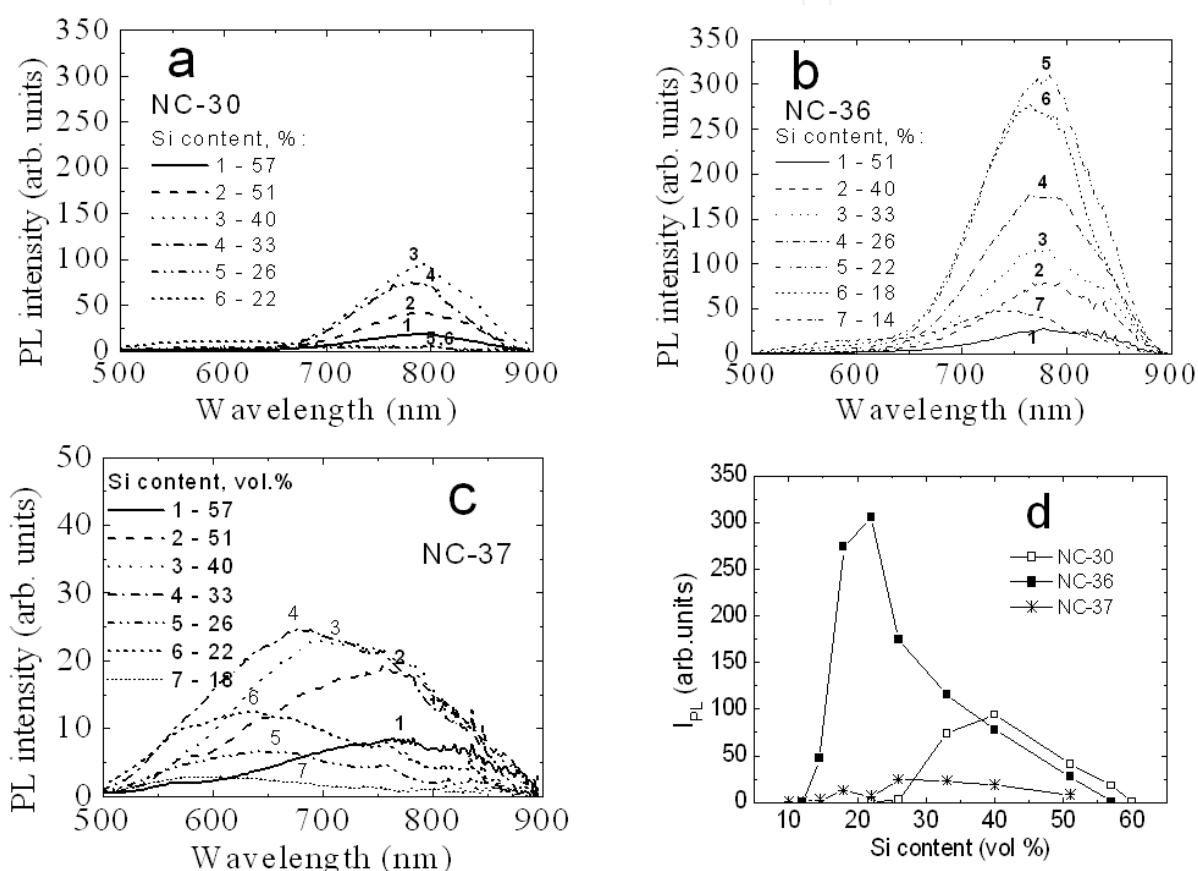


Fig. 8. PL spectra taken from samples with different Si contents: NC-30 (a), NC-36 (b) and NC-37(c). The results are summarized in graph (d), which shows the intensity of the most intense NC-related PL peak versus the Si content of oxide layers in samples NC-30 (785 nm), NC-36 (785 nm), and NC-37 (780 – 580 nm). (Antonova et al., 2009 a)

4.2 Charge storage capacity of irradiated NC:SiO₂ layers

The density of fixed oxide charges in the initial (non-irradiated) structure NC-30 and in the NC-SiO₂ layers of samples irradiated with Bi ions at different ion energies (NC-33, NC-34, NC-36) and at different ion fluences (NC-36, NC-37) versus the excess Si content of NC-SiO₂ layers is shown in Fig. 9 a, b. The data were extracted from measured C-V characteristics of MOS capacitors considering the flat-band voltage values. Note that prior to performing C-V measurements the irradiated samples were annealed at 800°C for 20 min with the aim to

remove irradiation-induced electrically active defects from the substrate. The sign of the oxide charge (capture of electrons or holes) was found to be dependent on the substrate conductivity type, which was altered during irradiation. The fixed charge in the NC-SiO₂ layer of sample NC-35 irradiated with the lowest ion fluence was low ($< 10^{12} \text{ cm}^{-2}$) due to the high compensation of the substrate.

An important observation discussed in Refs. (Antonova et al., 2006 b; 2008 b) consists in that a relatively high density of electrons trapped and stored at nanocrystals in NC-SiO₂ layers presents a peaking function of the excess Si content of the layers. A decrease in the fixed oxide charge that was observed in NC-SiO₂ layers with high Si phase contents was attributed to the formation of NC clusters in the oxide layer, resulting in impossibility for individual NCs to retain trapped charges. Further increase in NC concentration leads to the formation of conductive NC chains in turn giving rise to percolation conductivity. The peaking dependence of charge storage capacity of NC-SiO₂ layers on the excess Si content of these layers simply reflects the fact that the density of isolated NCs capable of retaining trapped charges goes through a maximum if considered as a function of excess Si content of the layers. The most striking finding here is that, within experimental accuracy, the maximum charge storage capacity of NC-SiO₂ layers was observed at exactly the same Si contents for which a maximum PL intensity coming from the NC-SiO₂ layers was registered. Variations in the deposition and/or annealing conditions of Si-rich oxide layers alter the proportion between the amounts of the excess silicon contained in Si nanocrystals and Si amorphous inclusions; as a result, the maximum in the curve of stored charge and versus the Si content of NC-SiO₂ layers and the maximum in the curve of NC-related PL intensity both exhibit shifts. It is significant, however, that in all cases a maximum charge storage capacity of NC-SiO₂ layers was observed in the same samples in which a maximal NC-emitted PL emission was registered. In (Antonova et al., 2008 b), a concept of delocalization threshold for an ensemble of NCs was introduced, this threshold being associated with the onset of substantial migration of charge carriers within NC clusters. This delocalization threshold is determined by both carrier migration and inter-cluster tunneling processes, and it corresponds to the excess Si content at which the PL and charge storage maxima are observed. Thus, a remarkable matching between the onset of the formation of quantum dot clusters, the above-discussed charge-storage and PL properties of NC systems, percolation-clusters theory and intra-cluster carrier migration processes was revealed.

We have found that in irradiated structures, in agreement with the suggested delocalization threshold concept, the maximum charge trapping at nanocrystals was observed exactly in the same region of excess Si contents in which a most intense PL emission from NCs was detected (compare Figs. 9 and 7, 8). Irradiation of the NC-SiO₂ layers with high-energy heavy ions results in widening of the range of layer compositions for which a substantial charge trapping by NCs is observed and in shifting the position of the charge storage maximum towards lower excess Si contents (Antonova et al., 2010 a; 2010 b). With the increase in ion energy, the range of Si contents of NC-SiO₂ layers in which additional charge could be accumulated at NCs also exhibited a shift towards lower Si contents. This finding, proving that additional NCs were formed in irradiated samples, well correlates with our PL and Raman data.

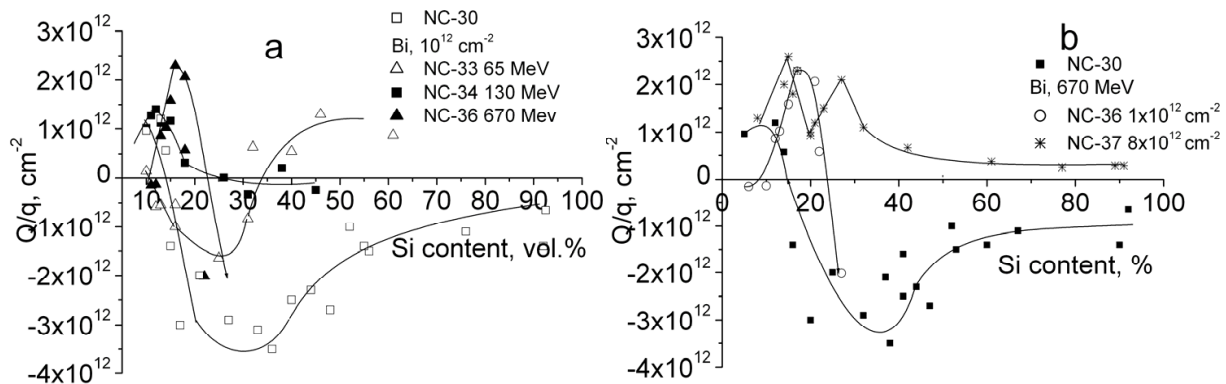


Fig. 9. The density of the NC-trapped charge as extracted from the flat band voltages of MOS capacitors versus the Si phase content of 400-nm thick NC-SiO₂ layers irradiated with Bi⁺ ions: with variation of (a) the ion energies for the ion fluence of 10¹² cm⁻², and (b) the ion fluencies for energy of 670 MeV. Irradiated regimes are indicated in the figures.

Observation of two peaks in the graph of Fig. 9 b for the sample irradiated with the highest ion dose correlates with the emergence of two peaks in Fig. 8 d in the curve for the same sample. Note that the high magnitude of the charge stored at NCs implies a high concentration of Si NCs formed due to irradiation in the range of relatively low Si contents of NC-SiO₂ layers. Thus, the higher the fluence, the higher is the NC concentration in the mentioned range of Si contents. With reference to Fig. 9, it can be hypothesized that the concentration of irradiation-induced Si NCs formed in NC-SiO₂ layers with a relatively low content of excess Si increases with increasing the ion fluence. The appearance of a dip at ~30% Si content in the dependence for the sample NC-37 (with simultaneous emergence of two peaking features on either side of the dip) can be attributed to the formation of NC clusters in the NC-SiO₂ layer with an increased concentration of irradiation-induced NCs. It should be noted here that the maximum value of the NC-stored charge for the data of Fig. 9 is ~3x10¹² cm⁻²; this value complies with the maximal density of isolated nanocrystals with sizes ~ 3-5 nm in NC:SiO₂ systems. One more interesting conclusion that can be drawn from a comparison of data in Figs. 9 b and 8 d is that the NC-related PL exhibits a more pronounced decrease with increasing NC concentration in comparison with NC charge storage capacity.

4.3 Transport properties and inter-cluster migration effects

In part of our samples with high Si content, percolation conduction was observed. For evaluating the conductivity of NC-SiO₂ layers, we measured I-V characteristics of reference and irradiated samples versus the Si-phase content. From such measurements, the curves of resistivity R of our NC:SiO₂ layers versus the Si content of those layers were deduced; these curves are shown in Fig. 10. For reference (non-irradiated) samples, a percolation transition with a percolation threshold at Si contents 33 - 40 vol.% was revealed; at this threshold, a sharp decrease in the resistivity of NC:SiO₂ layers amounting to about six orders of magnitude was observed. The position of the percolation threshold was found to be dependent on the proportion between the contents of crystalline and amorphous Si inclusions in the SiO₂ layer. The 33% position of the threshold, consistent with theoretical predictions (Shklovskii & Efros, 1984), was observed in NC:SiO₂ layers deposited at low

rates (Antonova et al., 2006 b). It was found that the percolation conduction threshold shifts to higher contents of excess Si in SiO_x layers after irradiation of the samples with high ion fluences ($\sim 10^{13} \text{ cm}^{-2}$) or with high-energy ions producing relatively weak ionization in the material. In those cases, as a rule, the conductivity of oxide layers in the interval of x -values above the percolation threshold decreased in magnitude in irradiated samples because of partial amorphization of Si nanocrystals, as supported by Raman data. In samples irradiated with relatively low fluences ($1 \times 10^{12} \text{ cm}^{-2}$) of 670 MeV Bi ions the resistivity of the NC: SiO_2 layers in the region over the percolation threshold decreased by two orders in comparison with non-irradiated samples.

The above results can be self-consistently interpreted as follows. The conductivity in the range of composition of NC- SiO_2 layers above the percolation threshold depended weakly on the Si-phase content of our layers both in irradiated and non-irradiated samples. This finding is consistent with the predictions of percolation theory (Shklovskii & Efros, 1984). However, the conductivity of irradiated sample NC-36 was almost two orders of magnitude higher than that of non-irradiated sample NC-30. This is believed to be due to a much higher conductivity of the percolation network due to NC chains formed along ion tracks and having identical orientations of atomic planes within the ordered NC chains.

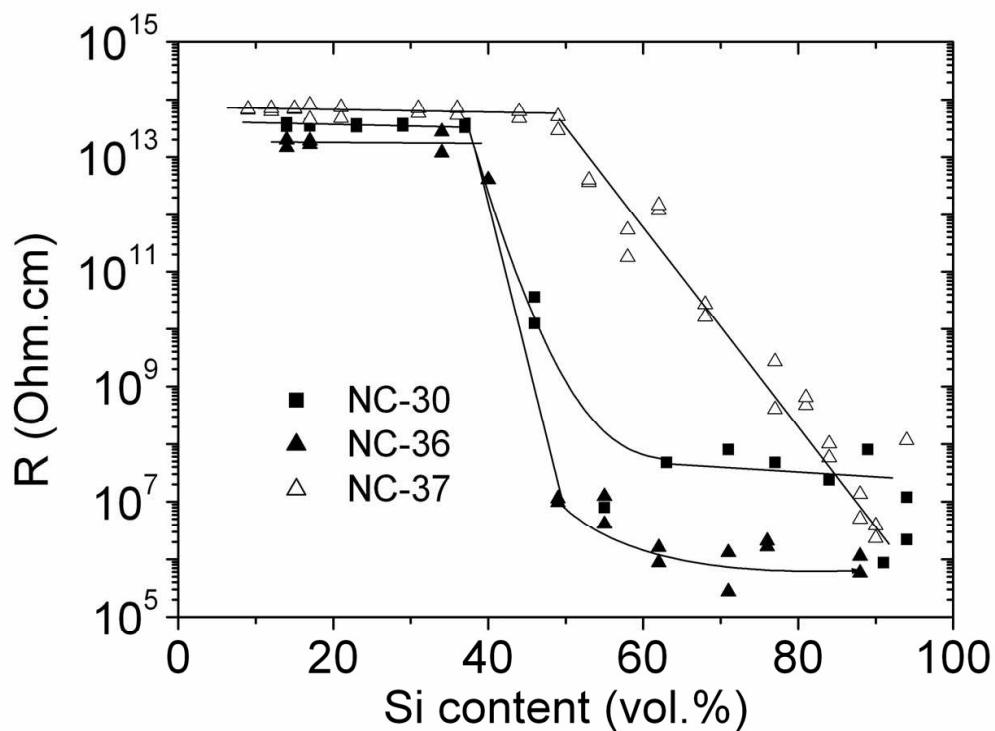


Fig. 10. The resistivity of NC: SiO_2 layers (measured at applied bias voltage 5 V) versus the Si phase content of the layers (vol.%) for reference sample NC-30 and for samples irradiated with 670 MeV Bi ions to fluences 10^{12} cm^{-2} (NC-36) and $8 \times 10^{12} \text{ cm}^{-2}$ (NC-37). (Antonova et al., 2009 a)

In view of a higher conductivity of crystalline Si phase in comparison with amorphous Si phase, a narrower percolation transition can be expected in samples containing a larger amount of Si crystallites formed in the oxide layer with a concomitant reduction of a-Si

phase content as evidenced by TEM images and Raman data. Thus, crystallization is found to predominantly proceed in samples with relatively low contents of excess Si. For the other part of our samples, with a higher Si content (about and above the percolation threshold), and for higher ion fluences, amorphization of Si nanocrystallites becomes a dominating process. However, the formation of a larger amount of Si crystallites fails to offer a reasonable explanation to the lower resistivity of sample NC-36 in comparison with sample NC-30 since the average conductivity of NC chains at high Si contents (above the percolation threshold) decreases weakly with increasing NC concentration.

5. Low-dimensional effects in ion-modified 3D NC arrays

Modification of NC-containing films (NC-11a, NC-23a, and NC-31a) with high-energy ion irradiation was found to lead to the appearance of capacitance peaks in the low-frequency capacitance-voltage characteristics of MOS capacitors formed on our samples. The *C-V* characteristics of reference and irradiated samples measured at different frequencies are shown in Fig. 11. As it is seen, two distinct capacitance peaks appear in the low-frequency *C-V* curve after irradiation. Such peaks were observed only in irradiated structures that contained 60–80% of excess silicon in 400–1000 nm thick NC:SiO₂ layer (Antonova et al., 2009 b). The amplitudes of those peaks increased with decreasing the measurement frequency, while the voltage position of the peaks remained essentially the same for all frequencies at which our measurements were performed. Moreover, the bias voltages at which the peaks were observed were quite reproducible in measurements performed at different points on the surface of one and the same sample. In particular, in all investigated samples one of the observed peaks was located at $V \approx 0$.

The amplitude of the capacitance peaks (peaks 1 and 2 in Fig. 11 b) plotted as a function of frequency is presented in Fig. 12. This frequency dependence of capacitance *C* is given by

$$C(\omega) = \frac{C_{\max}}{\sqrt{1 + (\omega\tau)^2}}, \quad (2)$$

where $\omega = 2\pi f$ (Shi et al., 2002; Panchaipetch et al., 2006). Hence, the frequency dependence of the peak amplitude allows one to estimate the time constant τ of the NC charging process. The τ values obtained by fitting the experimental *C*(ω) data (Fig. 12) with formula (2) were found to lie around 1.5×10^{-5} s and 5×10^{-6} s respectively for peaks 1 and 2. The value 1.5×10^{-5} s is in a fairly good correlation with the characteristic time of carrier emission from the ground state of NCs estimated for 300 K by means of Q-DLTS (see Fig. 6).

The bias-voltage dependences of the real (*G*) and imaginary (*C*) parts of the admittance of NC-23a films, which were irradiated with Xe ions and measured at 10-kHz frequency are shown in Fig. 13. As it follows from Fig. 11, this frequency is low enough for the capacitance peaks which we attribute to the charging of Si nanocrystallites, to emerge. The data in Fig. 13 suggest the possibility of dividing the observed peaks into two groups according to their bias positions (I and II). The voltage difference between the two groups is ~ 2.6 V, and the voltage difference between neighboring capacitance peaks within each group is roughly ~ 0.5 V. The *G-V* curves exhibit only two less pronounced peaks observed at the same voltages.

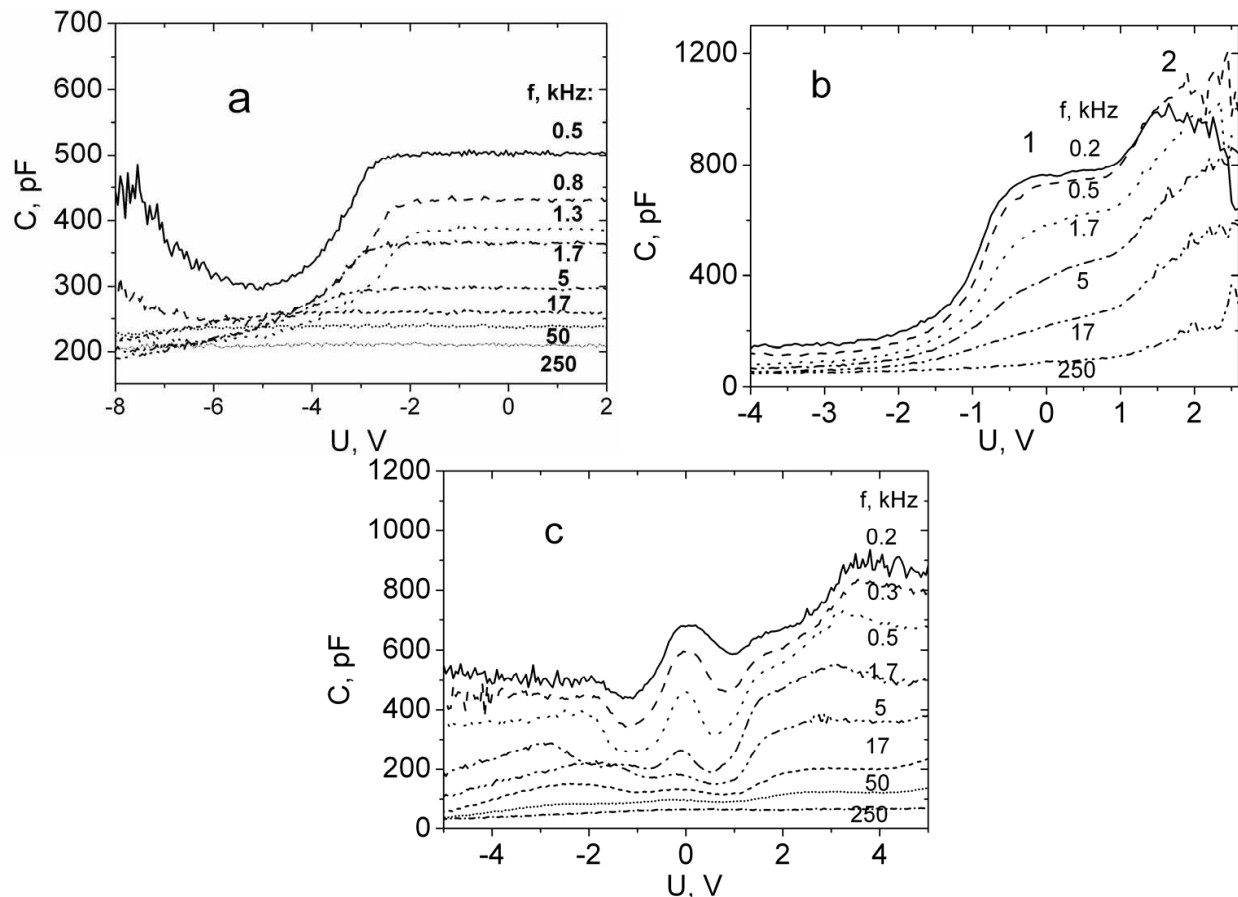


Fig. 11. C-V characteristics of NC-SiO₂ structures measured at room temperature and various frequencies for Si-phase contents 72% (a, b) and 79% (c) of oxide layer (initial sample NC-10 (a) and two samples from the sample series NC-11a irradiated with Kr ions (b, c). (Antonova et al., 2009 b)

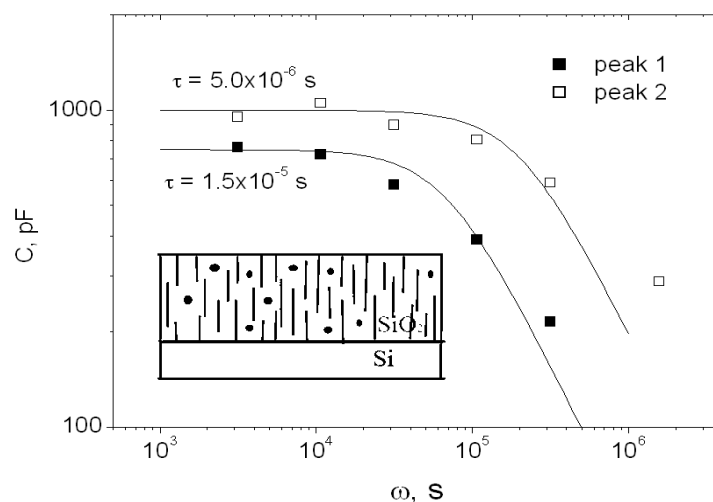


Fig. 12. The amplitudes of capacitance peaks 1 and 2 (Fig. 11 b) versus frequency. The peak numbers refer to the two main peaks in Fig. 11 b. The curves are the dependences that fit the τ values estimated from Q-DLTS data (symbols) with formula (2). The inset illustrates our model of NC chain formation in NC-SiO₂ layers subjected to high-energy ion irradiation. (Antonova et al., 2009 b)

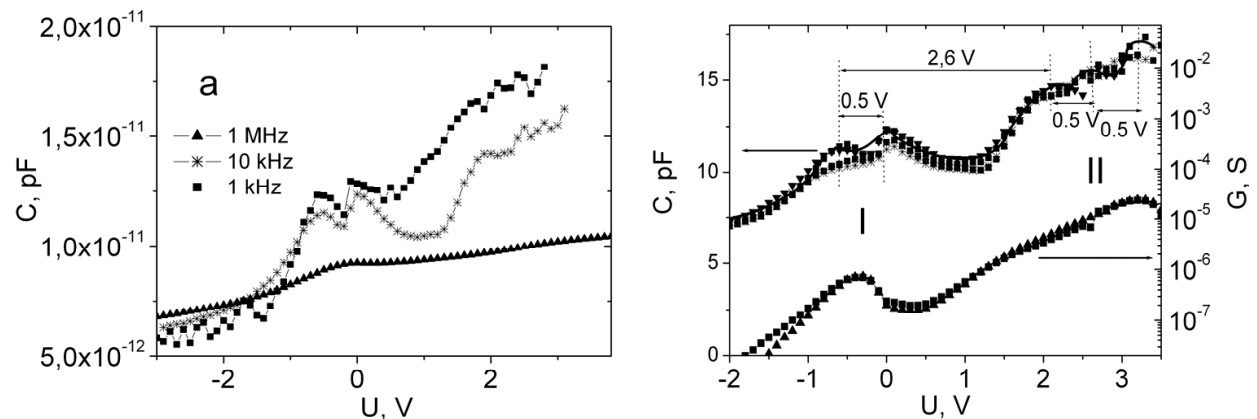


Fig. 13. Typical C-V and G-V characteristics of a MOS capacitor with Si NCs in the oxide layer (Si-phase content 63 vol.%) irradiated with Xe ions. Different points refer to different repeatedly performed measurements.

Similar peaks with similar characteristics were previously observed in C-V characteristics of thin (3–10 nm) oxide layers with an embedded two-dimensional array of Si NCs; the latter peaks were attributed to the charging process of electronic levels in NCs, and the voltage spacing between them (in V) was associated with the energy spacing (in eV) between the quantum confinement levels in NCs (Wu et al., 2004; Yu et al., 2005). It is significant that in our samples similar effects were observed for thick (400–1000 nm) NC-containing layers. We have suggested that the peaks could also be due to resonance tunneling of charge carriers to electronic levels in nanocrystals. This interpretation leans upon the fact that at high frequencies the electrons participating in the tunneling processes could not follow the voltage modulation, while at low frequencies they could respond to it; as a result, tunneling of charge carriers through the oxide into NCs could give rise to the capacitance peaks. A qualitative model to interpret the nature of the experimentally observed effect in ordered three-dimensional NC arrays is described below.

Taking into consideration our data (TEM, Raman spectroscopy, transport and C-V measurements, Q-DLTS), we suggest that radiation-induced NC chains were formed within ion tracks in our samples and that the peaks found in the C-V characteristics possibly reflected the formation of those NC chains. Considering the fact that the Si-phase content of the structures on which C-V measurements were performed (> 60%) was in a notable excess of the Si-phase content of the structures that were used in TEM study (35–40%) while the number of ion tracks in both cases was roughly identical, we suppose that, very likely, more pronounced NC chains were formed in our layers with the higher Si content. The lengths of those chains were approximately identical, defined by the thickness of the NC-SiO₂ layer. In samples with a Si content exceeding the percolation threshold those chains formed a conducting network. The NCs forming the chains were unable to retain the captured charge due to the high electric conduction existing between the NCs. So, only isolated NCs in non-conductive cells in the conducting network formed by NC chains could retain charge, the recharging of those NCs proceeding through the "bottlenecks" located between the isolated NC and neighboring chains. It is the charge trapping at such isolated Si nanocrystals that was probably responsible for the emergence of additional peaks in the C-V characteristics of irradiated samples. The effect due to resonance tunneling could be observed in such NC

systems because, here, the conducting network played the role of a “substrate” that created, together with a particular isolated NC, a two-barrier tunneling system in which the individual Si nanocrystal was separated from the “substrate” with a tunneling gap. Since the probability of tunneling through a barrier strongly (exponentially) depends on the barrier width, it can be assumed that the spread of tunnel-barrier widths involved in the phenomenon was rather small. Irrespective of the exact position of “bottlenecks” in the conducting NC chains, for statistical reasons the resistances of such chains and the resistances of the rest part of the NC cluster for different NC chains had close values and, as a result, the total bias voltage applied to the oxide was divided between each NC chain and the “bottleneck” in roughly identical proportions. Statistically, all the parallel NC chains involved tunneling gaps of roughly identical widths; as a result, NCs in different non-conductive cells can be expected to be recharged at roughly identical voltages. A sketch of QD chains formed along ion tracks in an irradiated sample is shown in the inset of Fig. 12. Charge carriers are captured by NCs at bias voltages at which resonant tunneling conditions are realized. In a real situation, the concentration N_{NC} of isolated NCs contributing to measured capacitance presents only a small fraction of the total NC concentration. In our case, all NC chains are connected in parallel and the total induced capacitance is therefore equal to the product $C_{\text{NC}}N_{\text{NC}}$. The magnitude of the capacitance peak ΔC is ~ 6 pF for the first group of NC-related capacitance peaks (Fig. 12). The capacitance of one NC is estimated as 8 aF (see below). Thus, we have $N_{\text{NC}} \approx 8 \times 10^8 \text{ cm}^{-2}$, this value constituting approximately 10^{-3} of the total number of all ion tracks (10^{12} cm^{-2}).

A more difficult problem here is interpretation of the bias voltage values of the C-V peaks. Let us try to correlate these values with characteristics of the resonant tunneling process and with the charging energies of a single NC. For that purpose, consider the τ values that were extracted from the $C(\omega)$ curves shown in Fig. 12. The probability T of carrier tunneling through the rectangular barrier between NCs as a function of the energy position of the levels in NC can be estimated using the expression

$$T = \exp\left(-\frac{2}{\hbar} \int_{x_2}^{x_1} p dx\right) \sim \exp\left(-\frac{d}{\lambda}\right), \quad (3)$$

where $p = \frac{h}{\lambda}$ is the carrier momentum, $\lambda = \frac{h}{\sqrt{2mE}}$ is the electron wavelength, and $d = x_1 - x_2$ is the width of the tunneling barrier between an isolated NC and the substrate or between an isolated NC and the adjacent NC chain, h is the Planck constant, and m is the electron effective mass in silicon. The tunneling being a dominating process, the tunneling time, or NC recharging time, is $\tau \sim T^{-1}$. In view of formula (3), the ratio τ_1/τ_2 (here, $\tau_1 = 1.5 \times 10^{-5}$ s and $\tau_2 = 5 \times 10^{-6}$ s, see above) can be expected to be a function of the quantum confinement energies in the NCs, so that

$$\ln\left(\frac{\tau_2}{\tau_1}\right) = \frac{h}{d\sqrt{2m}}(E_1^{-1/2} - E_2^{-1/2}). \quad (4)$$

Considering equation (1), we obtain a certain relation between τ_2/τ_1 and W . For the above-indicated values of τ_1 and τ_2 , the estimated NC diameter W is 3.3 nm assuming that the

tunneling distance is $d = 3$ nm. The value of W is in a very good agreement with the TEM values, 3-5 nm. This, then, suggests that, indeed, the capacitance peaks that we observed in the C-V characteristics can be associated with capture of electrons into quantum confined levels in NCs. Following the presented analysis, the first and the second groups of capacitance peaks in Figs. 11 and 13 can be associated with the charging of respectively the ground-state level and the first excited level in the NCs, whereas the relatively small peaks inside each group can be attributed to charging effects (Coulomb blockade energies) of NCs.

We have tested our model for consistency by performing an analysis typically used for NCs (Yu et al., 2005, Huang et al., 2003). The position of the photoluminescence peak observed in examined samples yields for the QD size a value 3.3 nm. The energy distance between the ground level and the first excited electronic level in such a QD is estimated to be $\Delta E = 103$ meV according to equation (1). The voltage difference between the two groups of peaks can be represented as $\Delta V = eK\Delta E$, where K is a coefficient depending on the geometry of the QD/matrix system. In the present case, we have $\Delta V = 2.6$ eV which value translates into $K=0.048$. The NC charging energy can be estimated from the relation $\Delta E_e = K\Delta V_e$; with the above value of K , this yields $\Delta E_e = 24$ meV. On the other hand, we have $\Delta E_e = e/C_{NC}$, where C_{NC} is the NC capacitance. The capacitance of an individual NC in our NC-SiO₂ layers was estimated as 8 aF, this value being quite a reasonable one for an NC ~ 3 nm in size.

6. Interaction of high-energy ions with silicon nanocrystals in dielectric matrix

Consider the processes that can be responsible for the radical transformations of NC arrays in ion-irradiated samples. First of all, it should be noted that the diffusivity of silicon in SiO₂ at temperatures 1110–1400°C is rather low, 10^{-21} – 10^{-17} cm²·s⁻¹ (Mathiot et al., 2003; Tsoukalas et al., 2001; Takahashi et al., 2003). According to the data of (De Almeida et al., 2000; Aleksandrov et al., 2008), oxygen possesses a much higher diffusivity in SiO₂ amounting to 10^{-9} – 10^{-7} cm²·s⁻¹. That is why the formation processes of Si nanocrystals in Si-rich oxide layers are usually described with consideration given to the fact that those processes should involve migration of oxygen atoms from the region of the growing silicon nanoparticle (see, for instance, Khomenkova et al., 2007). In addition, in their Monte-Carlo simulations, Muller et al. showed that the formation process of Si nanocrystals in Si:SiO₂ layers with a low excess Si content involves nucleation and growth of Si nanocrystals, whereas in Si:SiO₂ layers with a high excess Si content Si NCs are formed due to spinodal decomposition with separation of the Si and SiO₂ phases (Muller et al., 2002). Thus, it follows from the above consideration that, due to the local release of energy in ion tracks and the corresponding heating of the material there (see Fig.15 a, and Section 2.2, Fig.1 a), oxygen is bound to leave track regions, where Si nanocrystals may form. It should be mentioned here that the high ionization of material in track regions can be expected to most likely enhance the diffusivity of all atoms.

All of the above-mentioned processes can be enhanced by the anisotropic strain fields produced by anisotropic heating and by the atoms leaving the track regions (Van Dillen et al., 2005). It is believed that, on irradiation, the material expands in the direction normal to the ion track and contracts in the direction parallel to the track axis. The steady-state (residual) strain ϵ_{st} (the relative change in lattice distance) can be estimated as (Van Dillen et al., 2005)

$$\varepsilon_{st} = \exp(AF) - 1, \quad (5)$$

where A is the rate of strain accumulation in a material irradiated with a particular type of ions, and F is the ion fluence. The rate of strain accumulation can be estimated as

$$A = 0.463 \frac{1+\nu}{5-4\nu} \cdot \frac{\beta \frac{dE_e}{dx}}{\rho C}, \quad (6)$$

where ν is the Poisson's ratio, β is the coefficient of thermal expansion, ρ is the material density, and C is the specific heat. As follow from (6), the rate of strain accumulation A is proportional to the electronic losses of ions dE_e/dx . Invoking the well-known constants for SiO_2 ($\nu = 0.2$, $\beta = 5.5 \times 10^{-7} \text{ K}^{-1}$, $\rho = 2.2 \times 10^3 \text{ kg/m}^3$, $C = 10^3 \text{ J/kgK}$), we have estimated the strain accumulation rate A for the interval of ionization losses of used ions (see Fig. 14 a). For silicon, the quantity A has one and a half order of magnitude smaller value. For the case under consideration, using formula (5), we have also estimated the steady-state strain ε_{st} for ionization losses of ions ranging from 5 to 20 keV/nm. Those results are given in Fig.14 b. So, the strains in the layer are estimated as 3×10^{-5} – 8×10^{-3} depending on the ion used and on the ion fluence. This value is high enough for provoking significant strain-induced effects. The strain decreases with increasing the Si content in the NC: SiO_2 layer. This means that, at low Si contents, the diffusion flux of oxygen from track regions and, consequently, the formation process of nanocrystals should be more pronounced. Our experimental data fairly well agree with such considerations. In particular, the high strain has to limit the phase separation in ion tracks, thus decreasing the size of formed NCs. This effect was clearly observed by means of PL and Q-DLTS measurements (see Sections 3.3 and 4.1): the higher are the ionization losses, the higher is the strain, and the smaller is the typical NC size.

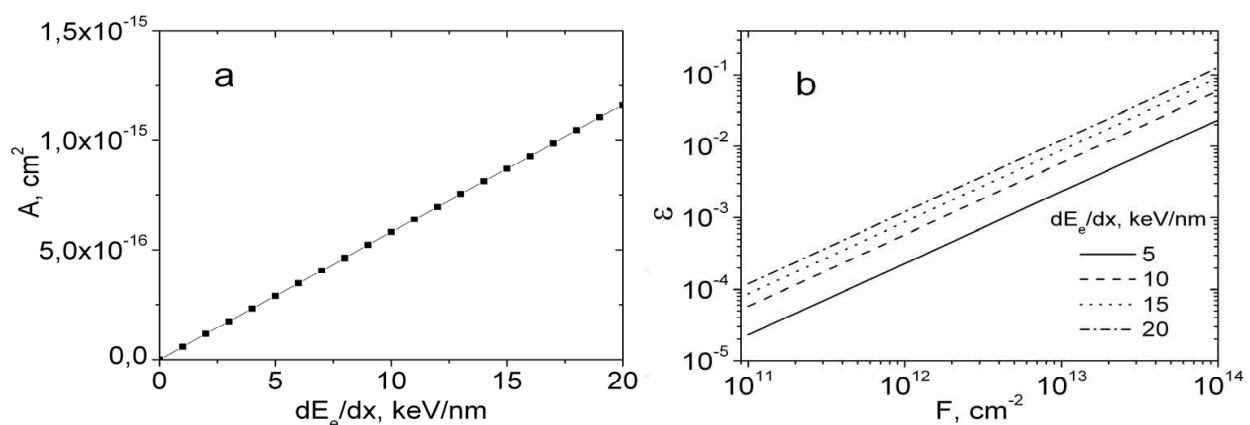


Fig. 14. (a) The strain accumulation rate A estimated for SiO_2 by formula (6) using constants $\nu = 0.2$, $\beta = 5.5 \times 10^{-7} \text{ K}^{-1}$, $\rho = 2.2 \times 10^3 \text{ kg/m}^3$, and $C = 10^3 \text{ J/kg}\cdot\text{K}$. (b) The steady-state strain ε_{st} estimated from (5) for different ionization losses of ions.

If the Si content of the SiO_2 layer is high, other processes control the interaction of high-energy ions with Si nanocrystals previously formed in SiO_2 . In this case, the interaction is defined by the relation between the nanocrystal diameter and the track diameter. With the example of Ge QDs, Schmidt et al. (Schmidt et al., 2007; 2009) showed that, if the nanocrystal size is such that the particles do not melt at a particular fluence, then the nanoparticles

change their spherical shape for an ellipsoidal one with increasing the ion fluence, and the sizes of nanoparticles in an ion track decrease in value along the track length. The mechanism of such a modification of nanoparticle shape is associated with the above-discussed anisotropic deformations of the particles. At the same time, the Si nanocrystals get amorphized and partially dissolved, as it was observed in (Mishra et al., 2007) and in the present study for samples with a high Si content. Nanoparticles smaller than, or comparable with, track dimensions are stretched along ion tracks. The threshold electronic losses corresponding to the onset of material melting in ion tracks in SiO₂ are thought to be 6 keV/nm (Meftah et al., 1997). Figure 15 presents a sketch illustrating the interaction of a high-energy ion with a nanocrystal. The crossing length of the NC of radius R by the ion track is $L_{nc} \leq 2R$. The nanocrystal will melt if the energy lost by the ion over the length L_{nc} exceeds the energy needed for melting the nanocrystal,

$$\frac{dE_e}{dx} L_{nc} \geq \frac{4\pi}{3} R^3 H_m \rho_{nc}, \quad (7)$$

where H_m is the melting heat and ρ_{nc} is the NC density. The maximal radii R of the nanocrystals in our samples which could be melted by the ions used in the present study are given in Table 3. For Kr, Xe, and Bi ions with energies 1–3 MeV/nucleon, melting occurs in all cases. As a result, nanocrystals elongated along ion tracks retain their crystal structure, whereas nanocrystals located in between ion tracks become amorphous. Integrally, these effects result in general ordering of nanocrystals along ion tracks. The same processes proceed in the case of metal inclusions embedded in an insulator matrix and, as it was shown recently (Mishra et al., 2007; Giulian et al., 2010; Dawi et al., 2011; Kumar et al., 2011), irradiation with sufficiently high ion fluences and energies provides a means for forming long wire-shaped nanoparticles in ion tracks.

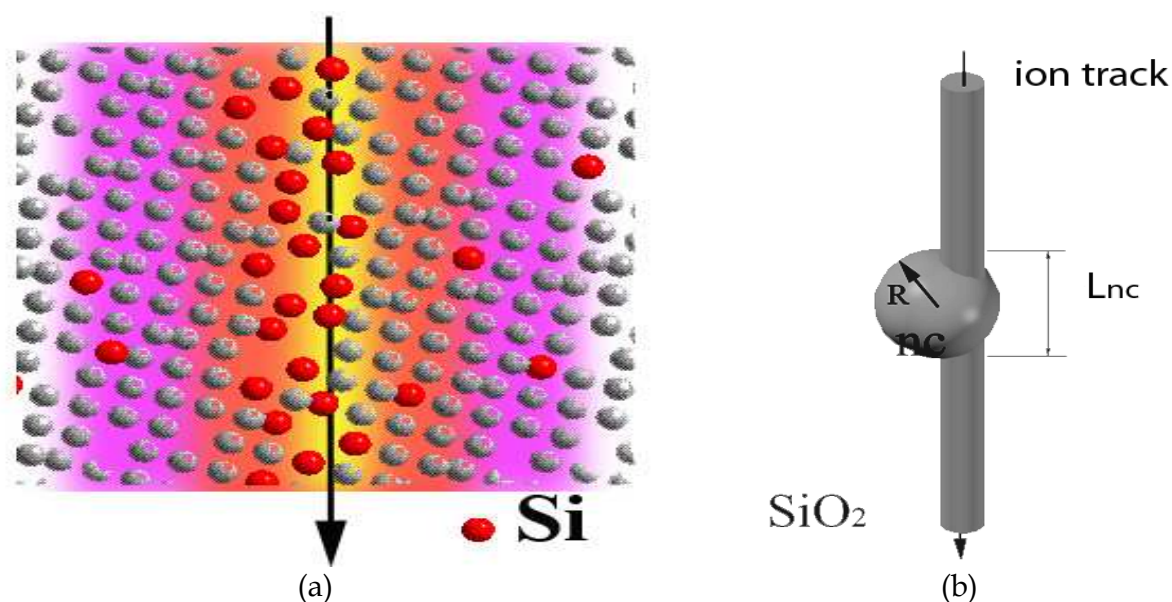


Fig. 15. (a) Sketch of an ion track in a composite crystal. Color gradient of the background is an illustration of the heating gradient. Non-uniform distribution of excess Si atoms (red balls) reflects the out-diffusion of oxygen from the track zone. (b) Sketch of the interaction of a high-energy ion with a nanocrystal.

Ion	Energy, MeV	dE_e/dx in Si, keV/nm	dE_e/dx in SiO ₂ , keV/nm	R, nm
Kr	90	8.0	7.1	≤40
Xe	130	12.3	10.5	≤43
Bi	65 - 670	9.1-23	7.9-18	≤50-68

Table 3. Maximal radii R of Si nanocrystals that could be melted by the used ions in ion tracks. Estimations were made with the use of inequality (7) and parameter values $\rho_{nc} = 2.33$ g/cm³ and $H_m = 164$ J/g.

7. Conclusions and outlook

As shown in this chapter, irradiation of Si:SiO₂ and NC:SiO₂ layers with high-energy heavy ions under the above-described conditions results in the formation of ordered low-dimensional NC systems that possess properties untypical of three-dimensional arrays of Si nanocrystals randomly distributed in the bulk of oxide layers. We have found that irradiation of our layers with heavy ions could either enhance or retard the formation of silicon nanocrystallites in the host matrix according to the irradiation dose used. We have also showed that both the electrical and optical properties of ion-irradiated layers could be improved by irradiating samples with low ion fluences. The increase of NC-emitted PL intensity and the extension of the interval of excess Si contents in which trapping of charges at NCs and emission of NC-related PL become detectable show much promise in applications of Si NCs. This suggests that, using a combination of properly chosen annealing and irradiation conditions, one can optimize the properties of NC:SiO₂ layers according to posed requirements. The ordering of Si nanocrystallites along ion tracks in oxide layers of irradiated samples leads to the formation of NC chain arrays. Moreover, the formed NCs have identically oriented atomic planes. Such NC systems cannot be obtained by other known NC formation methods. Other important features demonstrated by samples with NC chains thus formed in comparison with non-irradiated samples include: (1) high conductivity of the NC chains and (2) identical lengths of those chains, approximately equal to the oxide-layer thickness. Due to these features, the initial 3D system of QDs acquires properties of a low-dimensional array of QDs. Thus, irradiation of NC-SiO₂ layers with high-energy heavy ions enables the formation of new nanostructured materials exhibiting nontrivial structural and electronic properties not observed in materials produced by other technologies. The irradiation of NC-SiO₂ layers with high-energy heavy ions provides a useful tool that makes it possible to optimize the properties of NC arrays and fabricate vertically aligned nanostructures with low-dimensional properties.

Systems involving Si nanocrystals are of interest for a wide spectrum of applications, from solar cells to biomedical applications. The understanding of fundamental mechanisms that control the conductivity, the charge storage capacity, and the photoluminescence of nanocrystalline films modified with high-energy ions gives us the key to altering the properties of nanoscale materials in a desirable controlled manner and, in particular, the key

to solving the various problems encountered in applications of such materials. High-energy ion irradiation can be used as a tool for 3D structuring of composite materials allowing control of NC shape, size, and/or atomic plane orientation.

8. Acknowledgements

This study was supported by the Russian Foundation for Basic Research (Grant No. 11-02-92477).

9. References

- Aleksandrov, O.V., & Dusi, A.I., (1997). Model of Thermal Oxidation of Silicon at the Volume-Reaction Front. *Semiconductors*, Vol. 42, No. 11, (November 2008), pp. 1370-1376, ISSN 1063-7826.
- Antonova, I.V., Shaimeev, S.S. & Smagulova, S.A. (1997). Transformation of Electrically Active Defects as a Result of Annealing of Silicon Implanted With High-Energy Ions. *Semiconductors*, Vol. 40, No.5, (May 2006 a), pp. 543-548, ISSN 1063-7826.
- Antonova, I. V., Gulyaev, M.B., Yanovitskaya, Z. S., Volodin, V. A., Marin, D. V., Efremov, M. D., Goldstein, Y., & Jedrzejewski, J., (1997). Electrical Properties and Photoluminescence of SiO_x Layers with Si Nanocrystals in Relation to the SiO_x Composition. *Semiconductors*, Vol. 40, No. 10, (October 2006 b), pp. 1198-1203, ISSN 1063-7826.
- Antonova, I.V., Gulyaev, M.B., Skuratov, V.A., Marin, D.V., Zaikina, E.V., Yanovitskaya, Z.S., Jedrzejewski, J., & Balberg, I., (1988). Modification of Silicon Nanocrystals Embedded in an Oxide by High Energy Ion Implantation. *Solid State Phenomen.*, Vol.131-133, (2008 a), pp.541-546, ISSN 1012-0394.
- Antonova, I.V., Gulyaev, M.B., Savir, E., Jedrzejewski, J., & Balberg I. (1983). Charge Storage, Photoluminescence and Cluster Statistics in Ensembles of Si Quantum Dots. *Phys. Rev.B*, Vol. 77, No.12, (2008 b), 125318(5), ISSN 1098-0121.
- Antonova, I.V., Gulyaev, M.B., Volodin, V. A., Cherkov, A.G., Marin, D.V., Skuratov V.A., Jedrzejewski, J., & Balberg, I., (1990). Modification of Si Nanocrystallites Embedded in a Dielectric Matrix by High Energy Ion Irradiation. *Nanotechnology*, Vol.20, No.2, (February 2009 a), 095205(5), ISSN 0957-4484.
- Antonova, I.V., Kagan, M.S., Cherkov, A.G., Skuratov, V.A., Jedrzejewski, J., & Balberg, I., (1990). Low-Dimensional Effects in a Three-Dimensional System of Si Quantum Dots Modified by High-Energy Ion Irradiation. *Nanotechnology*, Vol.20, No.2, (April 2009 b), 185401(5), ISSN 0957-4484.
- Antonova, I.V., Neustroev, E.P., Smagulova, S.A., Jedrzejewski, V.A., & Balberg, I. (1991). Charge Spectroscopy of Si Nanocrystallites Embedded in a SiO₂ Matrix, *J. Appl. Phys.*, Vol. 106, No 6, (September 2009 c), 064306(6), ISSN 0021-7989.
- Antonova, I.V., Marin, D.V., Volodin, V. A., Skuratov, V.A., Jedrzejewski, J., & Balberg, I., (1988). Anisotropic Heating, Anisotropic Strain - Anisotropic Heating Engineering for Silicon Nanocrystals in SiO₂. *Solid State Phenomen.*, Vol.156-158, (2010 a), pp.523-528, ISSN 1012-0394.

- Antonova, I.V., Skuratov, V.A., Jedrzejewski, J., & Balberg, I., (1997). Ordered Arrays of Si Nanocrystals in SiO₂:Structural, Optical, and Electronic Properties, *Semiconductors*, Vol. 44, No. 4, (April 2010 b), pp. 482–487, ISSN 1063-7826.
- Antonova, I.V., Smagulova, S.A., Neustroev, E.P., Skuratov, V.A., Jedrzejewski, V.A., Savir, E., & Balberg, I. (1997). Charge Spectroscopy of SiO₂ Layers with Embedded Silicon Nanocrystals Modified by Irradiation with High_Energy Ions, *Semiconductors*, Vol. 45, No. 5, (May 2011), pp. 582–586, ISSN 1063-7826.
- Arnoldbik, W. M., Tomozeiu, N., van Hattum, E. D., Lof, R. W., Vredenberg, A. M., & Habraken, F. H. P. M. (1893). High-Energy Ion-Beam-Induced Phase Separation in SiO_x Films. *Phys. Rev.B*, Vol. 71, No. 12, (March 2005), 125329 (7), ISSN 1098-0121.
- Avasthi, D.K., Mishra, Y.K., Singh, F., & Stoquert, J.P. (1983). Ion Tracks in Silica for Engineering the Embedded Nanoparticles. *Nucl. Instrum. Methods Phys. Res. B*, Vol. 268, No.19, (October 2010), pp. 3027-3034, ISSN 0168-583X.
- Bitten, J.S., Lawis, N.S., Atwater, H.A., Polman, A. (1962). Size-Dependent Oxygen-Related Electronic States in Silicon Nanocrystals. *Appl. Phys. Lett.*, Vol. 84, No. 12, (June 2004), pp. 5389-5391, ISSN 0003-6951.
- Chaudhari, P. S., Bhawe, T. M., Kanjilal, D., & Bhoraskar, S. V. (1931) Swift Heavy Ion Induced Growth of Nanocrystalline in Silicon Oxide. *J. Appl. Phys.*, Vol. 93, No 6, (March 2003), pp. 3486-3489, ISSN 0021-7989.
- Chaudhari, P. S., Bhawe, T. M., Pasricha, R., Singh, F., Kanjilal, D., & Bhoraskar, S. V., (1983). Controlled Growth of Nanocrystallites in Silicon Oxide Matrix Using 150 Mev Ag Ion Irradiation. *Nucl. Instrum. Methods Phys. Res. B*, Vol.239, No.3, (August 2005), pp.185- 190, ISSN 0168-583X.
- D'Orleans, C.; Stoquert, J. P.; Estournes, C.; Cerruti, C.; Grob, J. J.; Guille, J. L., Haas, F.; Muller, D.; & Richard-Plouet, M. (1893). Anisotropy of Co Nanoparticles Induced by Swift Heavy Ions *Phys. Rev.B*, Vol. 67, No. 22, (June 2003), pp. 220101(4), ISSN 1098-0121.
- Dawi, E.A.; Vredenberg, A.M.; & Rizza, G.; Toulemonde, M. (1990). Ion-induced elongation of gold nanoparticles in silica by irradiation with Ag and Cu swift heavy ions: track radius and energy loss threshold. *Nanotechnology*, Vol. 22, No. 21, (May 2011), pp. 215607-215619, ISSN 0957-4484.
- De Almeida, R.M.C., Goncalves, S., Baumvol, J.R., & Stediler, F.C., (1893). Dynamics of Thermal Growth of Silicon Oxide films on Si. *Phys. Rev. B*, Vol. 61, No. 19, (May 2000), pp.12992-12999, ISSN 1098-0121.
- Fink, D.; Chadderton, L. T. ; Hoppe, K.; Fahrner, W. R. , Chandra, A.;& Kiv A, (1983). Swift-Heavy Ion Track Electronics (SITE). *Nucl. Instrum. Methods Phys. Res. B*, Vol.261, No.1-2, (August 2007), pp.727- 730, ISSN 0168-583X.
- Gaponenko, S.V., (1998). *Optical Properties of Semiconductor Nanocrystals*. Cambridge University Press, ISBN 0521582415, Cambridge, UK.
- Giulian, R., Kremer, F., Araujo, L. L., Sprouster, D. J., Kluth, P., Fichtner, P. F. P., Byrne, A. P., & Ridgway, M. C. (1893). hape transformation of Sn nanocrystals induced by swift heavy-ion irradiation and the necessity of a molten ion track. *Phys. Rev. B*, Vol. 82, No. 11, (September 2010), 113410 (4), ISSN 1098-0121.

- Godefroo, S., Hayne, M., Jivanescu, M., Stesmans, A., Zacharias, M., Lebedev, O. I., Van Tendeloo, G., & Moshchalkov, V. V. (2006). Classification and Control of the Origin of Photoluminescence from Si Nanocrystals. *Nature Nanotechnology*, Vol.3, No. 3, (March 2008), pp.174-178, ISSN 1748-3387.
- Gur, I., Fromer, N. A., Geier, M. L., Alivisatos, A. P. (1980). Air-Stable All-Inorganic Nanocrystal Solar Cells Processed from Solution. *Science*, Vol.310, (October 2008), pp.462-465, ISSN 0036-8075.
- Hu, C.-W., Chang, T.-C., Tu, C.-H., Chiang, C.-N., Lin C.-C., Lee, S.-W., Chang, C.-Y., Sze, S.M., & Tseng, T.-Y. (1974). Enhancement of NiSi Nanocrystal Formation by Incorporation of Ge Elements for Nonvolatile Memory devices. *J. Electrochem Soc.*, Vol.156, No 9, (July 2009), pp. H751 – H755, ISSN 0013-4651.
- Huang, S., Banerjee, S., Tung, T.T., Oda, S. (1931) Quantum Confinement Energy In Nanocrystalline Silicon Dots from High-Frequency Conductance Measurement. *J. Appl. Phys.*, Vol. 94, No.11, (September 2003), pp.7261-7665, ISSN 0021-7989.
- Iacona, F., Irrera, A., Franz, G., Pacifici, D., Crupi, I., Miritello, M. P., Presti, C. D., & Priolo, F. (1995). Silicon-Based Light-Emitting Devices: Properties and Applications of Crystalline, Amorphous and Er-Doped Nanoclusters. *IEEE Journal of Selected Topics in Quantum Electronics*, Vol.12, No 6, (Nov.-Dec. 2006) pp. 1596 – 1606, ISSN 1077-260X.
- Kachurin, G.A., Rebohle, L., Skorupa, W., Yankov, R.A., Tyschenko, I.E., Floeb, H., Boehme, T., Leo, K. (1997). Short-wavelength photoluminescence of SiO₂ layers implanted with high doses of Si⁺, Ge⁺, and Ar⁺ ions. *Semiconductors*, Vol. 32, No.4, (1998), pp. 392-396, ISSN 1063-7826.
- Kim, S.-K., Cho, C.-H., Kim, B.-H., Park, S.-J., & Lee, J. W. (1962). Electrical and Optical Characteristics of Silicon Nanocrystals Solar Cells. *Appl. Phys. Lett.*, Vol.95, No 14, (October 2009), 143120 (3), ISSN 0003-6951.
- Khomenkova, L., Korsunska, N., Stara, T., Venger, Ye., Sada, C., Trave, E., Goldstein, Y., Jedrzejewski, J., & Savir, E. (1967). Depth Redistribution of Components of SiO_x Layers Prepared by Magnetron Sputtering in the Process of Their Decomposition. *Thin Solid Films*, Vol. 515, No.17, (June 2007), pp.6749 – 6753, ISSN 0040-6090.
- Klaumunzer, S. (1983). Modification of Nanostructures by High-Energy Ion Beams. *Nucl. Instrum. Methods Phys. Res. B*, Vol.244, No.1, (March 2006), pp.1- 7, ISSN 0168-583X.
- Klimov, V. I., Ivanov, S. A., Nanda, J., Achermann, M., Bezel, I., McGuire, J. A., & Piryatins, A. (1969). Single-Exciton Optical Gain in Semiconductor Nanocrystals, *Nature* Vol. 447, (May 2007) pp.441 – 446, ISSN: 0028-0836.
- Kumar, H., Ghosh, S., Avasthi, D.K., Kabiraj, D., Mücklich, A., Zhou, S., Schmidt, H., & Stoquert, J.-P. (2006). Ion beam-induced shaping of Ni nanoparticles embedded in a silica matrix: from spherical to prolate shape. *Nanoscale Research Letters*, Vol. 6, No.1, (February 2011), 155 (9), SSN: 1556-276X.
- Mathiot, D., Schunck, J.P., Perego, M., Fanciulli, M., Normand, P., Tsamis, C., & Tsoukalas, D., (1931). Silicon self-diffusivity measurement in thermal SiO₂ by

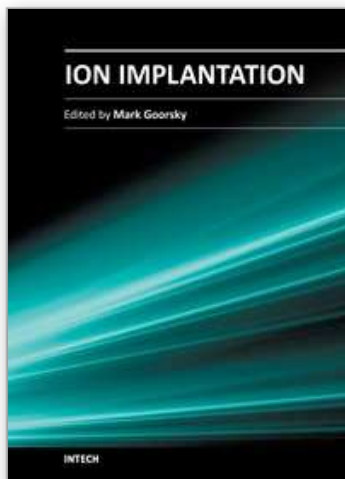
- $^{30}\text{Si}/^{28}\text{Si}$ isotopic exchange. *J. Appl. Phys.*, Vol. 94, No.3, (May 2003), pp.2136-2138, ISSN 0021-7989.
- Meftah, A., Brisard, F., Constantini, J.M., Dooryhee, E., Hage-Ali, M., Hervieu, M., Stoquert, J.P., Studer, F. & Toulemonde, M. (1993). Track Formation in SiO_2 Quartz and the Thermal-Spike Mechanism. *Phys. Rev.B*, Vol. 49, No. 18, (May 1997), pp. 12457-12463, ISSN 1098-0121.
- Michalet, X., Pinaud, F. F., Bentolila, L. A., Tsay, J. M., Doose, S., Li, J. J., Sundaresan, G., Wu, A. M., Gambhir, S. S. & Weiss, S., (1980). Quantum Dots for Live Cells, in Vivo Imaging, and Diagnostics. *Science*, Vol. 307, (January 2005), pp.538-544, ISSN 0036-8075.
- Mishra, Y.K., Singh, F., Avashthi, K., Pivin, J.C., Malinowska, D., & Pippel, E. (1962). Syntensis of elonged Au nanoparticles in silica matrix by ion irradiation, *Appl. Phys. Lett.*, Vol. 91, No. 6, (August 2007), 063103(3), ISSN 0003-6951.
- Moskalenko, A.S., Beracdar, J., Prokofiev, A.A., & Yassievich, I.N. (1993). Single-Particle States in Spherical Si/SiO_2 Quantum Dots. *Phys. Rev.B*, Vol. 76, No.8, (2007), 085427(9), ISSN 1098-0121.
- Muller, T., Heining, K.-H., & Moller, W. (1962). Size and Location Control of Si Nanocrystals at Ion Beam Synthesis in Thin SiO_2 Films. *Appl. Phys. Lett.*, Vol. 81, No 16, (August 2002), pp. 3049-3051, ISSN 0003-6951.
- Norris, D.J.; Efros, A.L.; & Erwin S.C. (1980). Doped Nanocrystals. *Science*, Vol.319, (March 2008), pp.1779-1779, ISSN 0036-8075.
- Punchaipetch, P., Ichikawa, K., Uraoka, Y., Fuyuki, T., Tomyo, A., Takahashi, E., & Hayashi, T. (1983). Experimental Investigation of Tunnel Oxide Thickness on Charge Transport Through Si Nanocrystal Dot Floating Gate Memories. *Vac. Sci. & Technol. B*, Vol. 24, No.3, (April 2006), pp. 1271-1277, ISSN 1071-1023.
- Rizza, G., Ramjauni, Y., Gacoin, T., Vieille, L., & Henry, S. (1993). Chemically Synthesized Gold Nanoparticles Embedded in a SiO_2 Matrix: a Model System to Give Insights into Nucleation And Growth Under Irradiation. *Phys. Rev. B*, Vol. 76, No.24, (December 2007 a), 245414 (9) , ISSN 1098-0121.
- Rizza, G., Chevery, H., Gacoin, T., Lamasson, A., & Henry, S. (1931) Ion Beam Irradiation of Embedded Nanoparticles: Toward an *in Situ* Control of Size and Spatial Distribution. *J. Appl. Phys.*, Vol. 101, No.1, (January 2007 b), 014321(7), ISSN 0021-7989.
- Rizza, G.; Dawi, A. E. A.; Vredenberg, M., & Monnet, I. (1962). Ion Engineering of Embedded Nanostructures: from Spherical to Facetted Nanoparticles. *Appl. Phys. Lett.*, Vol.95, No.4, (July 2009), 043105(3), ISSN 0003-6951.
- Sa'ar, A., Reichman, Y., Dovrat, M., Krapf, D., Jedrzejewski, J., & Balberg, I. (2001). Resonant Coupling between Surface Vibrations and Electronic States in Silicon Nanocrystals at the Strong Confinement Regime. *Nano Lett.* Vol.5, No.12, (November 2005), pp.2443-2447, ISSN 1530-6984.
- Schmidt, B., Mucklich, A., Rontzsch, L., & Heining, K.-H. (1983). How Do High Energy Ions Shape Ge Nanoparticle Embeded into SiO_2 ?, *Nucl. Instrum. Methods Phys. Res. B*, Vol. 257, No.1-2 , (April 2007) , pp. 30-32, ISSN 0168-583X.

- Schmidt, B., Heining, K.-H., Mucklich, A., & Akhmadaliev, C., (1983). Swift-heavy-ion-induced shaping of spherical nanoparticules into disks and rods. *Nucl. Instrum. Methods Phys. Res. B*, Vol. 267, No.8-9, (May 2009), pp. 1345-1348, ISSN 0168-583X.
- Shamin, S. N., Galakhov, V. R., Aksenova, V. I., Karpov, A. N., Shvartz, N. L., Yanovitskaya, Z. Sh., Volodin, V. A., Antonova, I. V., Ezhevskaya, T. B., Jedrzejewski, J., Savir, E., & Balberg, I. (1997). X-Ray and Infrared Spectroscopy of Layers Produced by Co-Sputtering of Spatially Separated SiO₂ and Si Sources. *Semiconductors*, Vol. 44, No. 4, (April 2010), pp. 531-536, ISSN 1063-7826.
- Shi, J., Wu, L., Huang, X., Liu, J., Ma, Z., Li, W., Li, X., Xu, J., Wu, D., Li, A. & Chen, K. (1963). Electron and Hole Charging Effect of Nanocrystalline Silicon in Double-Oxide Barrier Structure. *Solid State Commun.* Vol.123, (August 2002), pp. 437-442, ISSN: 0038-1098.
- Shklovskii, B.I., & Efros, A.L. (1984). *Electronic Properties of Doped Semiconductors*. Springer, ISBN-10 0387129952, Berlin, Germany.
- Takahashi, T., Fukatsu, S., Itoh, K., M., Uematsu, M., Fujiwara, A., Kageshima, H., Takahashi, Y., & Shiraishi, K., (1931). Self-Diffusion of Si in Thermally Grown SiO₂ under Equilibrium Conditions, *J. Appl. Phys.*, Vol. 93, No.6, (March 2003), pp. 3674-3676, ISSN 0021-7989.
- Toulemonde, M., Dufour, Ch., Meftah, A., Paumier, E. (1983). Transient Thermal Processes in Heavy Ion Irradiation of Crystalline, Inorganic Insulators. *Nucl. Instrum. Methods Phys. Res. B*, Vol.166-167, (May 2000), pp.903-912, ISSN 0168-583X.
- Tsoukalas, D., Tsamis, C., & Normand, P., (1931). Diffusivity Measurements of Silicon in Silicon Dioxide Layers Using Isotopically Pure Material. *J. Appl. Phys.*, Vol. 89, No.12, (March 2001), pp.7809 - 7813, ISSN 0021-7989.
- Van Dillen, T., Polman, A., Onck, P.R., & Van der Giessen, E. (1893). Anisotropic Plastic Deformation by Viscous Flow in Ion Tracks. *Phys. Rev.B*, Vol. 71, No. 2, (January 2005), 024103(12), ISSN 1098-0121.
- Van Dillen, T., de Dood, M.J.A., Penninkhof, J.J., Polman, A., Roorda, S., & Vredenberg, A.M, (1962). Ion Beam-Induced Anisotropic Plastic Deformation of Silicon Microstructures. *Appl. Phys. Lett.*, Vol. 84, No 18, (May 2004), pp.3591-3593, ISSN 0003-6951.
- Wu, L., Dai, M., Huang, X., Li, W., & Chen, K. (1983). Size-Dependent Resonant Tunneling and Storing of Electrons in a Nanocrystalline Silicon Floating-Gate Double-Barrier Structure. *J. Vac. Sci. & Technol. B*, Vol. 22, No.2, (March 2004), pp. 678-681, ISSN 1071-1023.
- Yu, L.W., Chen, K.J., Wu, L.C., Dai, M., Li, W., & Huang, X.F. (1893). Collective Behavior of Single Electron Effects in a Single Layer Si Quantum Dot Array at Room Temperature. *Phys. Rev. B*, Vol. 71, No. 24, (June 2005), 245305(5), ISSN 1098-0121.

Zhou, X., Uchida, K., & Oda, S. (1962). Current Fluctuations in Three-Dimensionally Stacked Si Nanocrystals Thin Films. *Appl. Phys. Lett.*, Vol. 96, No 9, (March 2010), 092112(3), ISSN 0003-6951.

IntechOpen

IntechOpen



Ion Implantation

Edited by Prof. Mark Goorsky

ISBN 978-953-51-0634-0

Hard cover, 436 pages

Publisher InTech

Published online 30, May, 2012

Published in print edition May, 2012

Ion implantation presents a continuously evolving technology. While the benefits of ion implantation are well recognized for many commercial endeavors, there have been recent developments in this field. Improvements in equipment, understanding of beam-solid interactions, applications to new materials, improved characterization techniques, and more recent developments to use implantation for nanostructure formation point to new directions for ion implantation and are presented in this book.

How to reference

In order to correctly reference this scholarly work, feel free to copy and paste the following:

Irina Antonova (2012). Si Nanocrystal Arrays Created in SiO₂ Matrix by High-Energy Ion Bombardment, Ion Implantation, Prof. Mark Goorsky (Ed.), ISBN: 978-953-51-0634-0, InTech, Available from: <http://www.intechopen.com/books/ion-implantation/si-nanocrystal-arrays-created-in-sio2-matrix-by-high-energy-ion-bombardment>

INTECH
open science | open minds

InTech Europe

University Campus STeP Ri
Slavka Krautzeka 83/A
51000 Rijeka, Croatia
Phone: +385 (51) 770 447
Fax: +385 (51) 686 166
www.intechopen.com

InTech China

Unit 405, Office Block, Hotel Equatorial Shanghai
No.65, Yan An Road (West), Shanghai, 200040, China
中国上海市延安西路65号上海国际贵都大饭店办公楼405单元
Phone: +86-21-62489820
Fax: +86-21-62489821

© 2012 The Author(s). Licensee IntechOpen. This is an open access article distributed under the terms of the [Creative Commons Attribution 3.0 License](#), which permits unrestricted use, distribution, and reproduction in any medium, provided the original work is properly cited.

IntechOpen

IntechOpen